Supporting Information for

Distal Conformational Locks on Ferrocene Mechanophores Guide Reaction Pathways for Enhanced Mechanochemistry

Yudi Zhang,[1†] Zi Wang,[1] Tatiana B. Kouznetsova,[1] Ye Sha,[2] Enhua Xu,[3] Logan Shannahan,[4] Muge Fermen-Coker,[4,*] Yangju Lin,[1] Chuanbing Tang,[2,*] Stephen L. Craig[1,*]

[1]Department of Chemistry, Duke University, Durham, North Carolina 27708, United States

[2]Department of Chemistry and Biochemistry, University of South Carolina, Columbia, South Carolina 29208, United States

[3]Graduate School of System Informatics, Kobe University, Kobe 657-8501, Japan

[4]US Army Research Laboratory, Maryland MD 21005, United States

Table of Contents

1. General Experimental Details

1.1 Materials

Ferrocene (98%), $LiAlH_4$ (95%), $AlCl_3$ (99%), n-BuLi solution (1.6M, in hexanes), potassium tert-butoxide (> 98%), 3-buten-1-ol (96%), N-(3-Dimethylaminopropyl)-N′-ethylcarbodiimide hydrochloride (EDCl, 98%), dimethylaminopyridine (DMAP, 98%), ethyl vinyl ether (EVE, 99%), Grubbs II catalysts (98%), 2,4,6-Tris(2-pyridyl)-*s*-triazine and 1,10-phenanthroline were purchased from Sigma-Aldrich and used as received. Acryloyl chloride (97%) and 9-oxabicyclo[6.1.0]non-4-ene (epoxy COD, 95%) was purchased from Sigma-Aldrich and freshly distilled before use. CO_2 (99.999%) was purchased from Airgas. [3]ferrocenophane and [5]ferrocenophane was synthesized according to literature.[1,2] All solvents were dried unless otherwise stated.

1.2 Characterization and methods

^{1}H NMR and ^{13}C NMR spectra were recorded on a 400 MHz or 500 MHz Varian NMR spectrometer using $CDCl_3$ as solvent. The chemical shifts are reported with respect to $CHCl_3/CDCl_3$(δ(1H) = 7.26 ppm, δ(13C) = 77.0 ppm). ESI-MS spectra were collected on an Agilent LC/MSD Trap instrument.

1.3 SMFS Measurements

As described below, details regarding the instrumentation, data acquisition, and experimental parameters for both constant velocity and force-clamping data are identical to those conducted previously by our group,[3,4] except that the solvent employed here was toluene. Specifically, a small (~10-20 μl) drop of diluted polymer solution (0.1-1 mg/ml

in tetrahydrofuran) was deposited on a substrate and allowed to evaporate. The volume of the polymer solution used was adjusted to ensure that, in general the AFM tip would successfully pick a polymer once per 10-100 attempts to reduce the odd of picking up multiple chains at once. After that sample was placed on an AFM stage, and the fluid cell was filled with toluene. The system was allowed to equilibrate for approximately 1 hour or until cantilever deflection drift was less than 1 pN/sec prior to conducting experiments.

All experiments were performed at ambient temperature (~23 °C) using homemade Atomic Force Microscopes, which are constructed of a Digital Instruments scanning head mounted on top of a piezoelectric positioner. Two types of cantilever probes with spring constants in the range of 20-30pN/nm were used: Sharp Microlever silicon probes (MSNL), and Silicon Nitride AFM probes (PNP-DB) were purchased from Bruker (Camarillo, CA) and NanoAndMore USA Corp (Watsonville, CA), correspondingly. The spring constants were calibrated for each probe in air, using the MFP-3D system (Asylum Research Group Inc., Santa Barbara, CA), applying the thermal noise method, based on the energy equipartition theorem as described previously. Force curves were collected on dSPACE (dSPACE Inc. Wixom, MI) and National Instruments (Austin, TX) hardware and analyzed using Matlab (The MathWorks, Inc., Natick, MA). All data were filtered during acquisition at 500 Hz. After acquisition, the data were processed and plotted using homemade software written in Matlab.

Constant velocity data were obtained as follows. The cantilever was repeatedly brought in contact with surface at different points with a scanning grid pattern with a force of ~5 nN. After it was held at rest for 2-5 seconds, the cantilever was withdrawn at a constant speed at 300 nm/sec to reduce hydrodynamic drag force. The signal from the photodetector was filtered with a low-pass filter at 500 Hz and data was collected at 5 kHz sampling rate.

1.4 Force-clamping experiments

The force clamp data were collected using a similar automated grid pattern as employed in the constant velocity experiments, with the exception that when the experimental apparatus detected a successful "catch" event (defined here as the pulling force reaching the threshold value of 650 - 800 pN for *cis*-3FCP and 750 - 900 pN for *cis*-5FCP, for a distance between probe and surface greater than 150 nm), it triggered a switch into the force clamp mode. Force clamping involves manipulating the AFM stage position relative to the probe via active feedback so as to maintain a constant, designated "clamp" force for up to 10 s or until the polymer chain detaches, whichever comes first. If the polymer chain did not detach during the 10 s "force clamp", force control was switched off, and the AFM stage was withdrawn with constant velocity. The force control feedback was implemented by Simulink model running on DS1104 control board. Cantilever deflection and AFM stage extension were recorded at a sampling rate of 5 kHz, and the photodetector signal low-pass filter was set to 2 kHz. Additional details have been published previously.[3]

1.5 PDMS specimen preparation and mechanical testing

Procedures were adopted from previously reported literature.[5] Generally, Sylgard 184 Base (2.0 g) was added to a 20 mL scintillation vial followed by 0.2 mL of a 75 mg/mL solution of *cis*-3FCP diene (compound **1**) and diallyl 1,1'-ferrocenedicarboxylate[6] in xylenes. The solution was mixed thoroughly with a vortex mixer until completely dispersed. 0.2 g curing agent was added subsequently, and the mixture was further mixed extensively with a vortex mixer. The solution was degassed for 30 min, poured into a cylindrical Teflon mold or rectangular PTFE film mold and cured in an oven at 65 □ overnight.

The obtained PDMS specimen was then swollen in a phenanthroline solution (20 mg/mL in dichloromethane, DCM) or 2,4,6-Tris(2-pyridyl)-*s*-triazine (TPTZ) solution (15 mg/mL in DCM) overnight. Then the sample was quickly washed with DCM to remove residual phenanthroline on the surface and dried at room temperature under vacuum overnight.

A 20 mm diameter ID dry pressing die set was purchased from Across International and used to conduct the drop test. The as-prepared silicone specimen (~ 6 mm in height) was sandwiched between the support table and the push rod. A weight was released freely from a certain height and allowed to hit the push rod. Split Hopkinson pressure bar test was performed on mechanophore embedded silicone specimen using methods reported previously.[7] Specifically, the sample is placed between two polycarbonate bars. A coaxially aligned projectile is fired using a gas gun into the end of one bar, which generates an elastic stress pulse. The pulse then travels through the sample and into the second bar. The wave speed of the polycarbonate was 1821 m/s and all experiments were carried out at a consistent firing pressure of 30 psi.

1.6 Sonication experiments

Pulsed ultrasound experiments were conducted on Vibracell Model VCX50 sonicator at 20 kHz with a 12.8 mm replaceable tip titanium probe from Sonics and Materials. Sonication was carried out on 2 mg/mL polymer solutions in THF immersed in an ice/water bath. The solutions were degassed in nitrogen for 30 min before sonication and a continuous N_2 stream was bubbled through the solution throughout the sonication process. Pulsed ultrasound was performed at a power of 8.7 W/cm^2 and the sonication sequence was set as 1s on 1s off.

2. Synthesis

2.1 Small molecule synthesis

2.1.1 Synthesis of *cis*-[3]ferrocenophane diene (1) and *trans*-[3]ferrocenophane diene (2)[8]

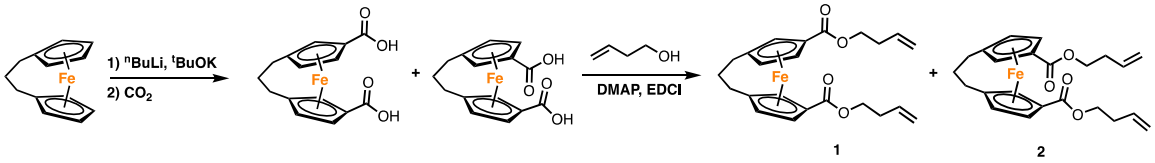

[3]ferrocenophane[1] (52 mg, 2.3 mmol) and ^{t}BuOK (0.77 g, 6.9 mmol) was dissolved in anhydrous hexane in a dry round bottle. *n*-BuLi solution (1.6M in hexane, 4.3 mL, 6.9 mmol) was put in an addition funnel and 5 mL hexane. The mixture was added dropwise to the round bottle and react for overnight under room temperature. On the second day, red precipitates were formed, and the mixture was cooled to -78 □. CO_2 was purged continuously to the mixture for 2h until the mixture turned from red to yellow. Then the reaction was carefully quenched with 25 mL water. The water layer was washed with benzene for 2 times while the organic layer was washed with water for 2 times. After washing, water layer was combined and precipitated with 1M HCl solution. Yellow precipitates were collected through filtration, dried under vacuum for overnight and used directly for next step.

The mixture of acids (40.53 mg, 1.3 mmol) were dissolved in 100 mL anhydrous DCM, 3-buten-1-ol (0.68 mL, 7.8 mmol), DMAP (32 mg, 2.6 mmol) and EDCl (1.5 g, 7.8 mmol) was added subsequently. The mixture was allowed to stir for 2 days. Then 50 mL water was added to the mixture. Organic layer was washed with water for 3 times, combined and dried with anhydrous $MgSO_4$. Then the mixture was purified by flash column chromatography (ethyl acetate: hexane=1:9 as eluent). The product **1** was obtained as a red oil (25 mg, 46% yield). ^{1}H NMR (400 MHz, $CDCl_3$) δ = 5.89-5.79 (m, 2H), 5.17-5.06 (m, 4H), 4.81 (d, 2H), 4.19 (t, 4H), 4.15 (t, 2H), 2.45 (dtd, 4H), 2.04-1.89

(m, 6H). ^{13}C NMR (500 MHz, $CDCl_3$) δ = 169.56, 134.46, 117.06, 89.39, 74.75, 73.02, 71.83, 71.09, 63.29, 35.00, 33.33, 24.18. EI-MS: (m/z): 423 (M^+, 100%). The product **2** was obtained as an orange oil (4 mg, 7% yield). ^{1}H NMR (400 MHz, $CDCl_3$) δ = 5.90-5.82 (m, 2H), 5.18-5.09 (m, 4H), 4.61 (d, 2H), 4.53 (m, 2H), 4.40 (m, 2H), 4.29-4.19 (m, 4H), 2.49-2.45 (dd, 4H), 1.97 (m, 6H). ^{13}C NMR (500 MHz, $CDCl_3$) δ = 170.78, 134.37, 117.26, 89.59, 73.81, 73.58, 71.66, 63.50, 35.04, 33.40, 29.85, 24.15. EI-MS: (m/z): 423 (M^+, 100%).

2.1.2 Synthesis of *cis*-[3]ferrocenophane macrocycle (3)

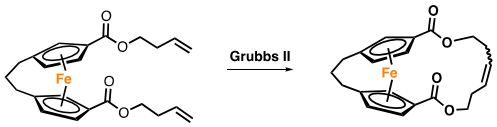

Cis-[3]ferrocenophane diene (**1**, 57.5 mg, 0.136 mmol) was dissolved in 70 mL anhydrous DCM and purged with argon for 15 min. Grubbs II catalyst (11.6 mg, 0.0136 mmol) was then added as a solid, and the reaction was heated to 40 □. 1 mL of ethyl vinyl ether was added to quench the reaction after 5 h. The solvent was removed, and the mixture was purified by flash column chromatography (ethyl acetate: hexane=1:3 as eluent). The product was further purified by recrystallization from ethyl acetate/hexane (v/v=1:5) and obtained as a red crystal (44 mg, 82% yield). ^{1}H NMR (400 MHz, $CDCl_3$) δ = 5.63 (td, 2H), 4.77 (d, 4H), 4.29 (ddd, 2H), 4.17-4.09 (m, 4H), 2.34 (q, 2H), 2.02-1.89 (m, 6H). ^{13}C NMR (500 MHz, $CDCl_3$) δ = 170.14, 129.30, 89.11, 76.04, 72.02, 71.55, 70.61, 63.98, 34.61, 30.89, 24.19. EI-MS: (m/z): 395 (M^+, 100%)

2.1.3 Synthesis of *trans*-[3]ferrocenophane macrocycle (4)

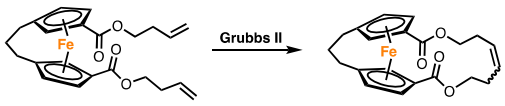

Trans-[3]ferrocenophane diene (**2**, 65 mg, 0.154 mmol) was dissolved in 80 mL anhydrous DCM and purged with argon for 15 min. Grubbs II catalyst (11.6 mg, 0.0136 mmol) was then added as a solid, and the reaction was heated to 40 □. 1 mL of ethyl vinyl ether was added to quench the reaction after 5 h. The solvent was removed, and the mixture was purified by flash column chromatography (ethyl acetate: hexane=1:3 as eluent). The product was further purified by recrystallization from ethyl acetate/hexane (v/v=1:5) and obtained as an orange crystal (44 mg, 82% yield). ^{1}H NMR (400 MHz, $CDCl_3$) δ = 5.57-5.55 (t, 2H), 4.65-4.64 (t, 2H), 4.51-4.50 (dd, 2H), 4.45-4.39 (m, 4H), 3.99-3.94 (td, 2H), 2.50-2.36 (m, 4H), 1.97 (m, 6H). ^{13}C NMR (500 MHz, $CDCl_3$) δ = 171.60, 128.90, 89.76, 73.52, 73.41, 72.77, 72.02, 63.82, 34.96, 31.52, 24.20. EI-MS: (m/z): 395 (M^+, 100%)

2.1.4 Synthesis of *cis*-[5]ferrocenophane diene (5)

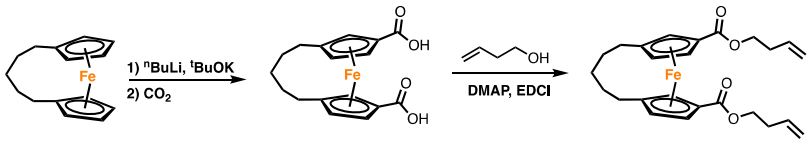

[5]ferrocenophane[2] (760 mg, 3.0 mmol) and potassium tert-butoxide (1.09 g, 9.0 mmol) were suspended in 25 mL Et_2O under argon at - 78 °C. The n-butyllithium (5.63 mL of 1.6 M solution in hexane, 9.0 mmol) was added dropwise and the solution turned dark red. The reaction proceeded at room temperature for 3 h, cooled to -78 °C, and CO_2 was bubbled overnight. The resulting crude suspension was diluted with 100 mL water and washed three times with 100 mL hexane. 50 mL of 2 M HCl solution was dropwise, leading to the precipitation of a yellow solid that was subsequently washed with DI water. Mixture of acids were collected as a yellow solid (765 mg, 75% yield).

The diacid mixture (300 mg, 0.88 mmol), 3-buten-1-ol (0.39 mL, 4.39 mmol), EDCl (1.0 g, 5.28 mmol) and DMAP (197 mg, 1.76 mmol) were dissolved in 20 mL DCM, the

flask of which was flame-dried and filled with nitrogen. The reaction proceeded at room temperature for 2 days. After reaction, the solvent was evaporated and the crude product was separated by silica gel column chromatography (polarity of mobile phase increased gradually from pure hexane to EtOAc : hexane = 1:19). Product was collected as a red oil (220 mg, 56% yield). ^{1}H NMR (400 MHz, $CDCl_3$) δ=5.91-5.80 (m, 2H), 5.17-5.07 (m, 4H), 4.81 (s, 2H), 4.71 (s, 2H), 4.26-4.22 (m, 4H), 4.16 (s, 2H), 2.48-2.43 (m, 4H), 2.53-2.29 (m, 4H), 2.23-2.16 (M, 2H), 1.85-1.82 (m, 4H) ; ^{13}C NMR (400 MHz, $CDCl_3$) δ=169.70, 134.43, 116.86, 92.57, 73.45, 71.36, 70.97, 69.55, 63.16, 33.18, 24.57, 24.56, 24.32. EI-MS: (m/z): 451 (M^+, 100%).

2.1.5 Synthesis of *cis*-[5]ferrocenophane macrocycle (6)

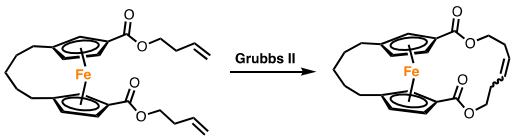

Cis-[5]ferrocenophane diene (**5**, 160 mg, 0.355 mmol) and Grubbs II catalyst (18.4 mg, 0.02 mmol) were dissolved in 200 mL anhydrous DCM in a nitrogen-filled, dry flask. The reaction proceeded at 40 °C overnight and several drops of ethyl vinyl ether were added to quench the reaction. Then the solvent was evaporated and the crude product was separated by silica gel column chromatography (polarity of mobile phase increased gradually from pure hexane to EtOAc : hexane = 1: 4). Subsequent recrystallization with EtOAc and hexane gave a red crystal (105 mg,70 % yield)**.** ^{1}H NMR (400 MHz, $CDCl_3$) δ=5.75-5.72 (m, 2H), 4.81(dd, J = 1.6, 1.2 Hz, 2H), 4.69 (t, J = 1.2 Hz, 2h), 4.33-4.21 (m, 4H), 4.19 (dd, J = 1.6 Hz, 1.2 Hz, 2H), 2.36-2.33 (m, 8H), 2.33 (s, 2H), 1.90-1.71 (m, 4H) ; ^{13}C NMR (400 MHz, $CDCl_3$) δ=170.43, 129.16, 92.29, 74.33, 71.29, 71.06, 69.82, 63.84, 30.66, 25.02, 24.59, 24.43. EI-MS: (m/z): 423 (M^+, 100%).

2.2 Polymer synthesis

2.2.1 Synthesis of *cis*-[3]ferrocenophane-*co*-epoxy COD (7)

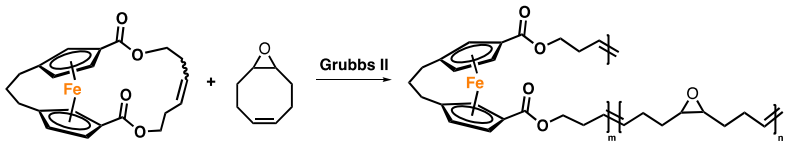

Cis-[3]ferrocenophane macrocycle (**3**, 12mg, 0.03 mmol) and epoxy-COD (16 mg, 0.13 mmol) was dissolved in 0.2 mL anhydrous DCM. The solution was purged with argon for 15 min. 0.01 mL of Grubbs II solution in DCM (0.4 mL, 20 mg/mL) was added to initiate the polymerization. After the reaction mixture was stirred at room temperature overnight, several drops of EVE were added to stop polymerization. The polymer solution was precipitated into methanol 3 times. The polymer was collected by filtration and dried under high vacuum overnight. Product **7** was obtained as a yellow solid (22 mg, 80%).

2.2.2 Synthesis of *trans*-[3]ferrocenophane-*co*-epoxy COD (8)

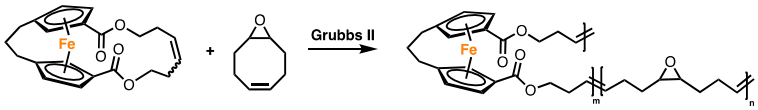

Trans-[3]ferrocenophane macrocycle (**4**, 6 mg, 0.015 mmol) and epoxy-COD (17 mg, 0.14 mmol) was dissolved in 0.2 mL anhydrous DCM. The solution was purged with argon for 15 min. 0.01 mL of Grubbs II solution in DCM (0.4 mL, 21 mg/mL) was added to initiate the polymerization. After the reaction mixture was stirred at room temperature overnight, several drops of EVE were added to stop polymerization. The polymer solution was precipitated into methanol 3 times. The polymer was collected by filtration and dried under high vacuum overnight. Product **8** was obtained as a yellow solid (16 mg, 70% yield).

2.2.3 Synthesis of *cis*-[5]ferrocenophane-*co*-epoxy COD (9)

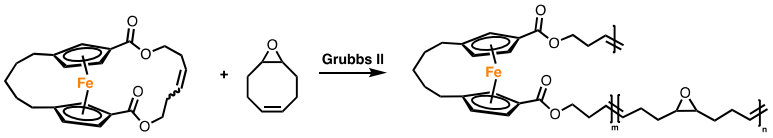

Cis-[5]ferrocenophane macrocycle (**6**, 20 mg, 0.047 mmol) and epoxy-COD (7 mg, 0.06 mmol) were dissolved in 0.15 mL anhydrous DCM. The solution was purged with argon for 15 min. 0.01 mL of Grubbs II solution in DCM (0.4 mL, 13 mg/mL) was added to initiate the polymerization. After the reaction mixture was stirred at room temperature overnight, several drops of EVE were added to stop polymerization. The polymer solution was precipitated into methanol 3 times. The polymer was collected by filtration and dried under high vacuum overnight. Product **9** was obtained as a yellow solid (20 mg, 75% yield).

2.2.4 Synthesis of *cis*-[3]ferrocenophane-*co*-ferrocene-*co*-epoxy COD (10)

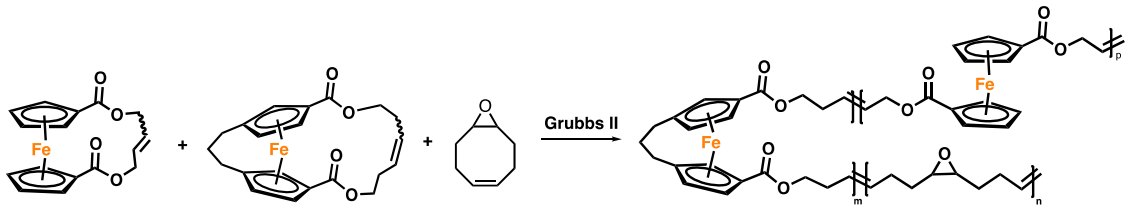

Cis-[3]ferrocenophane macrocycle (**6**, 16 mg, 0.04 mmol), ferrocene macrocycle (13.2 mg, 0.04 mmol) and epoxy-COD (25.2 mg, 0.2 mmol) were dissolved in 0.2 mL anhydrous DCM. The solution was purged with argon for 15 min. 0.02 mL of Grubbs II solution in DCM (0.4 mL, 6 mg/mL) was added to initiate the polymerization. After the reaction mixture was stirred at room temperature overnight, several drops of EVE were added to stop polymerization. The polymer solution was precipitated into methanol 3 times. The polymer was collected by filtration, dried under high vacuum for overnight. Product **10** was obtained as a yellow solid (46 mg, 84% yield).

2.2.5 Synthesis of *cis*-[3]ferrocenophane-*co*-*g*DCC (11)

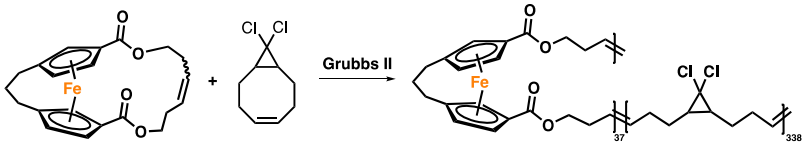

Cis-[3]ferrocenophane macrocycle (**3**, 12mg, 0.03 mmol) and gDCC-cyclooctene (42 mg, 0.22 mmol) were dissolved in 0.2 mL anhydrous DCM. The solution was purged with argon for 15 min. 0.01 mL of Grubbs II solution in DCM (0.4 mL, 20 mg/mL) was added to initiate the polymerization. After the reaction mixture was stirred at room temperature for 3 h, several drops of EVE were added to stop polymerization. The polymer solution was precipitated into methanol 3 times. The polymer was collected by filtration and dried under high vacuum overnight. Product **11** was obtained as a yellow solid (43 mg, 80%).

2.2.6 Synthesis of ferrocene-*co*-[4.2.0]bicyclooctene-*co*-*g*DCC (12)

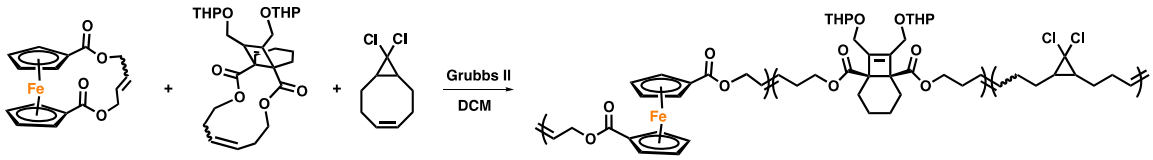

Ferrocene macrocycle (3 mg, 0.009 mmol), [4.2.0]bicyclooctene[18] (BCOE, 27 mg, 0.054 mmol) and *g*DCC-COD (26 mg, 0.14 mmol) were dissolved in 0.2 mL anhydrous DCM. The solution was purged with argon for 15 min. 0.02 mL of Grubbs II solution in DCM (0.4 mL, 8.5 mg/mL) was added to initiate the polymerization. After the reaction mixture was stirred at room temperature for 3 h, several drops of EVE were added to stop polymerization. The polymer solution was precipitated into methanol 3 times. The polymer was collected by filtration and dried under high vacuum overnight. Product **12** was obtained as a yellow solid (38 mg, 68% yield).

3. Sonication

Polymer **12** (30 mg, 4.5% FC, 15% BCOE) was dissolved in 15 mL THF and subjected to sonication for 30 min. The ^{1}H NMR spectra were obtained before and after the sonication and was stacked as shown below. The new peaks formed after sonication as highlighted below indicate the activation of both ferrocene and BCOE. The activation ratios of them were calculated based on the integration of the highlighted peaks and determined to be ~2% for ferrocene and ~5% for BCOE.

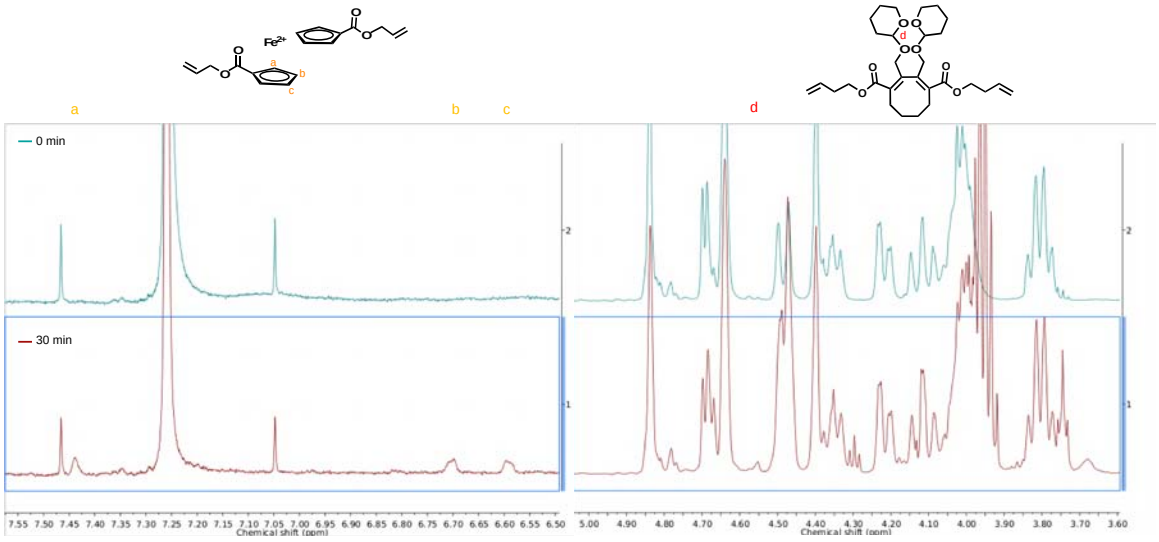

Figure 1. ^{1}H NMR spectra of **12** before (green) and after (red) the sonication. Peaks at ~7.45, 6.70, 6.60 ppm correspond to the activated ferrocene; peak at ~4.55 ppm correspond to the activated BCOE.

4. Single molecule force spectroscopy

4.1 SMFS fits for *cis*-[3]ferrocenophane-*co*-epoxy COD

Table 1. Parameters obtained for *cis*-[3]ferrocenophane

Entry	x[a]	*f**	$x^{\ddagger}$ (nm) BE	$x^{\ddagger}$ (nm) cusp	L_1(nm)	L_2(nm)	L_2/L_1	Kuhn Length	$E_{initial}$	E_{final}
1	0.18	817.5	0.073	0.249	427.8	513.4	1.20	0.34	2.5E+04	7.6E+04
2	0.18	784.3	0.076	0.260	359.7	434.3	1.21	0.41	1.7E+04	5.5E+04
3	0.18	838.2	0.074	0.249	300.8	374.6	1.24	0.33	2.1E+04	5.7E+04
4	0.18	821.5	0.073	0.251	379.7	444.2	1.17	0.43	1.7E+04	3.0E+04
5	0.18	799.6	0.074	0.252	515.2	584.3	1.13	0.30	2.8E+04	5.4E+04
6	0.18	841.4	0.073	0.243	186.4	224.2	1.20	0.30	3.0E+04	1.2E+05
7	0.18	766.9	0.075	0.256	423.7	510.5	1.20	0.36	2.1E+04	5.2E+04
8	0.18	819.0	0.078	0.254	205.8	235.9	1.15	0.32	2.8E+04	5.1E+04
9	0.18	781.2	0.074	0.254	335.3	428.8	1.28	0.52	9.5E+03	3.8E+04
10	0.18	783.7	0.080	0.264	182	205.1	1.13	0.24	5.8E+04	1.3E+05
11	0.12	779.5	0.081	0.272	260.9	282.6	1.08	0.17	7.9E+04	7.5E+04
12	0.12	827.3	0.081	0.266	105	107	1.02	0.16	2.2E+05	6.7E+04
13	0.12	826.6	0.073	0.250	414.5	468.4	1.13	0.35	2.9E+04	5.3E+04

[a]Molar ratio of the mechanophore determined by ^{1}H NMR.

4.2 SMFS fits for *trans*-[3]ferrocenophane-*co*-epoxy COD

Table 2. Parameters obtained for *trans*-[3]ferrocenophane

Entry	x[a]	*f**	$x^{\ddagger}$ (nm) BE	$x^{\ddagger}$ (nm) cusp	L_1(nm)	L_2(nm)	L_2/L_1	Kuhn Length	$E_{initial}$	E_{final}
1	0.07	1156.4	0.059	0.184	324.1	350.2	1.08	0.46	2.7E+04	5.0E+04
2	0.07	1154.5	0.060	0.181	344.1	368.5	1.07	0.44	3.2E+04	7.2E+04
3	0.07	1113.5	0.063	0.191	178.7	185.9	1.04	0.43	2.5E+04	2.9E+04
4	0.07	1154.8	0.061	0.185	400.7	419.4	1.05	0.40	4.9E+04	4.9E+04
5	0.07	1123.1	0.061	0.183	185.8	201.6	1.08	0.40	6.4E+04	6.4E+04
6	0.07	1201.2	0.062	0.184	264.2	274.6	1.04	0.35	5.9E+04	5.9E+05
7	0.07	1122.0	0.059	0.180	219.6	236.8	1.08	0.41	6.4E+04	6.4E+04
8	0.07	1117.3	0.062	0.186	317.2	337.1	1.07	0.42	5.5E+04	5.5E+04

[a]Molar ratio of the mechanophore determined by ^{1}H NMR.

4.3 SMFS fits for cis-[5]ferrocenophane-*co*-epoxy COD

Table 3. Parameters obtained for *cis*-[5]ferrocenophane

Entry	x[a]	*f**	$x^{\ddagger}$ (nm) BE	$x^{\ddagger}$ (nm) cusp	L_1 (nm)	L_2 (nm)	L_2/L_1	Kuhn Length	$E_{initial}$	E_{final}
1	0.21	965.7	0.075	0.241	308.4	330.0	1.08	0.16	9.9E+04	1.3E+05
2	0.21	944.8	0.084	0.242	324.5	389.2	1.19	0.17	4.3E+04	8.9E+04
3	0.30	1020.0	0.079	0.225	274.4	330.0	1.20	0.19	1.0E+05	1.8E+05
4	0.30	968.4	0.085	0.229	284.6	347.7	1.22	0.19	8.5E+04	1.7E+05
5	0.30	925.3	0.081	0.234	406.2	505.9	1.24	0.29	3.8E+04	9.2E+04
6	0.40	968.5	0.105	0.233	127.0	160.1	1.26	0.19	1.0E+05	2.7E+05
7	0.40	915.2	0.111	0.240	269.8	360.6	1.34	0.26	4.6E+04	1.2E+05

[a]Molar ratio of the mechanophore determined by ^{1}H NMR.

4.4 SMFS fits for *cis*-[3]ferrocenophane-*co*-ferrocene-*co*-epoxy COD

Table 4. Parameters obtained for *cis*-[3]ferrocenophane-*co*-ferrocene-*co*-epoxy COD

Entry	L_1(nm)	L_2(nm)	DP	# of ferrocene units[a]	Kuhn Length	$E_{initial}$	E_{final}
1	201.3	210.5	174.5	22.4	0.41	2.2E+04	2.0E+04
2	194.4	206.0	170.7	21.6	0.40	1.9E+04	2.1E+04
3	257.6	289.6	240.0	28.6	0.46	1.6E+04	3.4E+04
4	251.0	280.0	232.0	27.9	0.37	2.0E+04	4.2E+04
5	522.3	579.9	480.6	58.0	0.35	2.6E+04	5.1E+04
6	364.1	391.1	324.2	40.4	0.32	2.9E+04	3.3E+04
7	124.4	137.0	113.6	13.8	0.34	2.3E+04	4.6E+04
8	275.3	307.4	254.8	30.6	0.50	1.5E+04	3.3E+04
9	329.3	361.3	299.5	36.6	0.43	1.7E+04	3.0E+04
10	102.0	102.5	85.0	11.3	0.23	6.0E+04	3.4E+04
11	358.4	365.4	302.9	39.8	0.28	3.2E+04	2.2E+04
12	196.6	213.3	176.8	21.8	0.41	1.7E+04	2.5E+04
13	302.8	326.6	270.7	33.6	0.24	5.1E+04	8.0E+04

14	197.6	228.4	189.3	21.9	0.40	1.5E+04	4.5E+04
15	524.4	554.4	459.5	58.2	0.38	2.0E+04	2.2E+04
16	188.7	206.8	171.3	20.9	0.28	3.7E+04	6.5E+04
17	304.2	343.5	284.7	33.8	0.40	2.0E+04	4.9E+04
18	173.3	180.5	149.6	19.2	0.18	6.9E+04	7.5E+04
19	393.3	462.2	383.1	43.6	0.36	1.6E+04	5.6E+04
20	132.0	142.3	117.9	14.6	0.30	3.4E+04	5.4E+04
21	109.2	118.2	98.0	12.1	0.29	3.8E+04	7.4E+04
22	419.1	450.4	373.3	46.5	0.29	3.3E+04	6.1E+04

[a]Number of forrocene units is calculated as follows:

$$\#\ \text{of ferrocene unit} = \frac{L_{initial} \times x_{FC}}{L_{cis-3FCP} \times x_{cis-3FCP} + L_{FC} \times x_{FC} + L_{epoxy-COD} \times x_{epoxy-COD}}$$

where x denotes the molar fraction of various monomers within the polymer as determined by ^{1}H-NMR spectroscopy, and L refers to the force-free end-to-end distance obtained from CoGEF calculations (see section 9 for details) for the various monomers. $L_{initial}$ refers to the initial polymer contour length before transition.

5. Force-coupled reaction rates obtained from SMFS experiments

5.1 SMFS of unbridged ferrocene-containing polymers

In order to compare the force-coupled reaction rates of ferrocene and *cis*-3FCP, multiple *cis*-3FCP (12 %) and ferrocene (11 %) units were incorporated along the same polymer backbone (10) and probed by SMFS.

The rate-detachment force relationships of 7 and 10 were obtained by a spreadsheet-based method reported previously.[10] The chain scission/detachment rate $k_d(F)$ is defined as the probability of an event over a given time interval at a given force:

$$k_d(F) = N(F)/t(F)$$

where $N(F)$ is the number of events that occur at a given force F and $t(F)$ is the time that the bond spends at that force. $t(F)$ is calculated by multiplying the number of points in each force interval by $1/\nu$, ν is the sampling rate. If taking the statistical presence of multiple ferrocenes along the trapped polymer chain into account, $N(F)$ need to be divided by number of ferrocenes per chain as calculated in Section 4.4. As seen in Figure 2b, the upper limit for unbridged ferrocene dissociation is $15 \pm 3\ s^{-1}$ at forces of 1250 pN (Figure 2b). Because ***cis*-3FCP** mechanophores have already dissociated prior to reaching 1250 pN, we extrapolate the observed rate-force relationship at lower forces to obtain a force-coupled rate constant of $1.3 \times 10^5\ s^{-1}$ at 1250 pN, which is four orders of magnitude higher than the upper limit of ferrocene (and likely a couple orders of magnitude greater still).

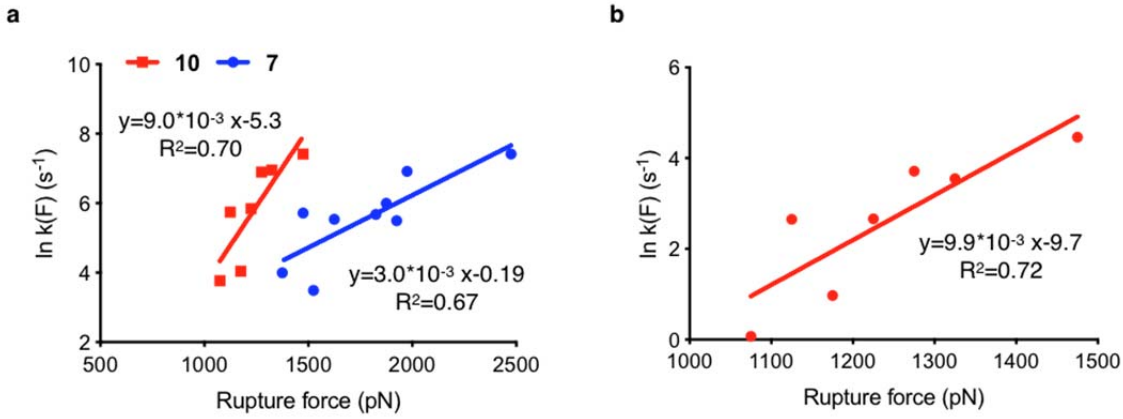

Figure 2. (a) Rate-force data for chain scission/detachment of **7** (blue) and **10** (red) with linear regressions. (b) Rate-force data for ferrocene dissociation taking the statistical presence of multiple ferrocenes along the trapped polymer chain into account.

5.2 Rate-force relationship obtained by force-clamping experiments [3]

Elongation of the polymer as a function of time was measured as shown in Figure 3. Extension data obtained in the force clamp regime were fitted with a single exponential decay function in Matlab using Levenberg-Marquardt nonlinear least squares algorithm as shown in Figure 4, which yields the effective first order rate constant c at a given force. The extracted rate constants at given forces for *cis*-3FCP and *cis*-5FCP were summarized in Table 5 and 6.

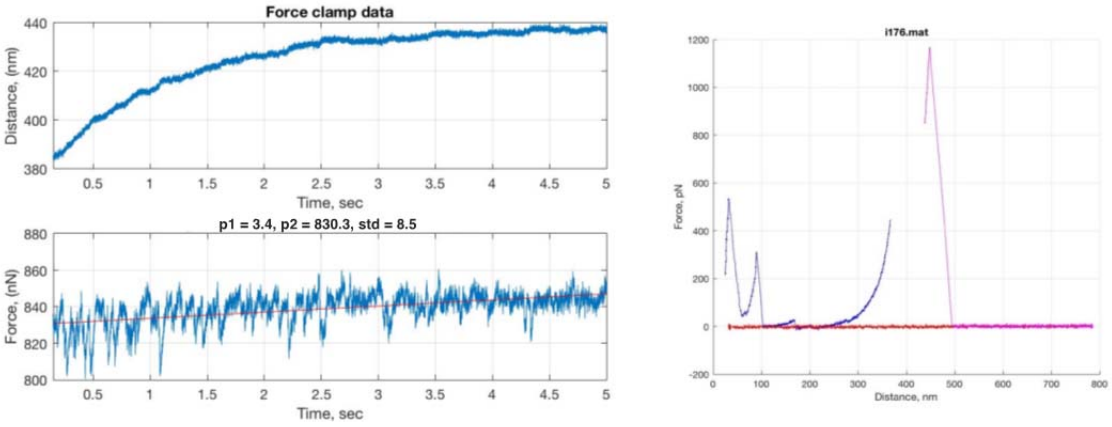

Figure 3. Representative data of force clamp experiments. The figure on the left shows data collected during time interval when force was held at a constant value. The figure on the right shows corresponding constant velocity data before and after force control engagement.

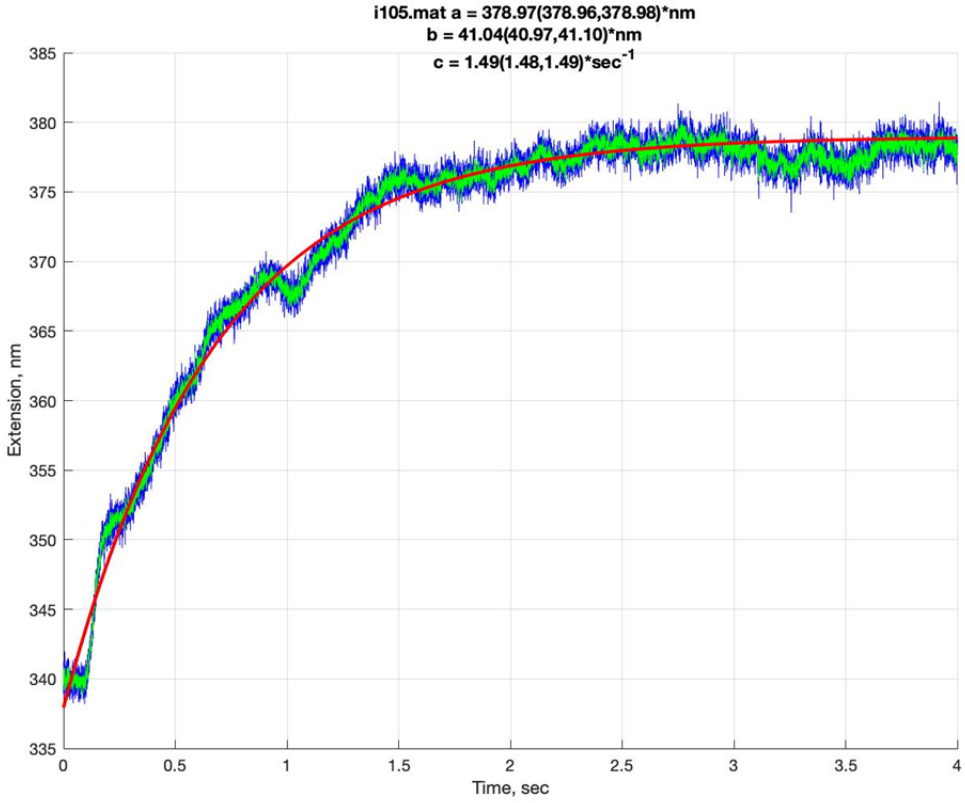

Figure 4. Representative data of a force clamp experiment. The blue trace represents the raw data and green trace represents the smoothed data using LOWESS regression smoothing method. Red line represents the single exponent fit of the smoothed data: $y = a - b * e^{-c*x}$ (a is final polymer contour length, b the polymer extension and c the reaction rate constant).

Table 5. Results of fitting force clamp extension data of *cis*-3FCP with single exponent $y = a - b * e^{-c*x}$ (a is the final polymer contour length, b is the polymer extension and c is the reaction rate constant).

Entry	Force (pN)	c (s^{-1})	ln(c)
1	683	0.994	-0.006
2	711	1.181	0.166
3	726	1.724	0.545
4	691	1.130	0.122
5	704	1.067	0.0651
6	762	1.985	0.685
7	660	0.155	-1.865
8	678	0.432	-0.839
9	785	2.593	0.953
10	719	1.393	0.332
11	733	1.510	0.412
12	771	2.126	0.754
13	765	2.232	0.803
14	758	2.472	0.905
15	707	0.682	-0.382
16	710	0.742	-0.298

Table 6. Results of fitting force clamp extension data of *cis*-5FCP with single exponent $y = a - b * e^{-c*x}$ (a is the final polymer contour length, b is the polymer extension and c is the reaction rate constant).

Entry	Force (pN)	c (s^{-1})	ln(c)
1	871	1.210	0.191
2	869	1.420	0.351
3	830	0.899	-0.106
4	811	0.488	-0.716
5	818	0.598	-0.514
6	815	0.526	-0.642
7	819	0.599	-0.513
8	772	0.321	-1.135
9	770	0.194	-1.639
10	796	0.479	-0.736
11	838	0.500	-0.694
12	851	1.255	0.227
13	863	2.082	0.733
14	856	0.510	-0.673
15	891	4.645	1.536

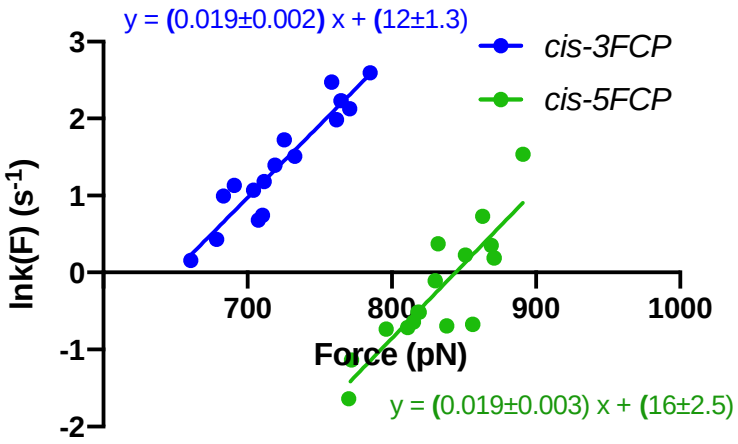

Figure 5. Summary of data from Table 5 and 6. Force coupled dissociation rates vs force obtained from force-clamping experiments for *cis*-3FCP (blue) and *cis*-5FCP (green). Blue and green straight lines are linear fits with Bell-Evans model. The critical uncertainty taken into account the experiment-to-experiment error and not includes the uncertainty of individual data point.

5.3 Summary of SMFS parameters

SMFS parameters obtained by fitting the constant velocity and force-clamping data with Bell-Evans model are summarized in Table 7.

Table 7. SMFS Parameters Obtained by Modeling Force-Extension Curves with Bell-Evans Model

Entry	Force clamping		$\Delta G^{\ddagger}$ (kcal/mol)[a]	Constant velocity	
	$\Delta x^{\ddagger}$ (Å)	k_0 (s^{-1})		$\Delta x^{\ddagger}$ (BE) (Å)	k_0 (s^{-1})
cis-3FCP	0.77±0.08	5.29E-6	24.8	0.76±0.03	9.41E-6
trans-3FCP	-	1.20E-6	25.7	0.69±0.01	2.09E-7
cis-5FCP	0.81±0.10	6.69E-8	27.4	0.88±0.14	9.50E-8

[a] Force-free activation energy are obtained by extrapolating rate-force data collected from force clamping experiments to F = 0 N.

5.4 Force-coupled rate for BCOE at 1250 pN

$\Delta x^{\ddagger}$ and $\Delta G^{\ddagger}$ were obtained from prior reports.[18]

The force free rate constant is calculated as:

$$k_0 = \frac{k_B T}{h} e^{\frac{-\Delta G^{\ddagger}}{RT}} = 6.21\text{E}12 * e^{\frac{-35.7*1000*4.182}{8.314*298}} = 4.1\ \text{E-}14\ s^{-1}$$

The rate constant at F = 1250 pN is calculated from a Kauzmann-Eyring model:

$$k(F) = k_0 e^{\frac{F\Delta x^{\ddagger}}{k_B T}} = 4.1 * 10^{-14} * e^{\frac{1250*e^{-12}*0.89*e^{-10}}{1.38e^{-23}*298}} = 2.4\ \text{E-}2\ s^{-1}$$

6. Determination of force-free rate constants

6.1 Ring strain calculation

Table 8. Force free activation energy calculated for ferrocene and ferrocenophanes

Entry	Tilt angle	Ring strain (kcal/mol)[a]	$\Delta G_0^{\ddagger}$ (model, kcal/mol)	$\Delta G_0^{\ddagger}$ (thermal, kcal/mol)
FC	0	0	-	54.8[11]
2FCP	21.6[12]	12.1	42.7	<46[c]
3FCP	7.6[13]	2.8	52.0	-
5FCP	1.7[b]	0.7	54.1	-

[a] Calculated by adapting the total energy-tilt angle relationship from literature.[14]

[b] Structure used was optimized by DFT.

[c] Estimated from reported thermodynamic data from literature.[15,16]

6.2 Force-free rate constant of *cis*-3FCP

At elevated temperature, *cis*-3FCP will isomerize to *trans*-3FCP and decompose as a result of Fe-Cp bond breakage (decomposition rate constant: k_1). The activation energy of

$$\textit{cis}\text{-3FCP} \xrightarrow{k_1} \text{decomposition}$$

this reaction gives a lower limit of *cis*-3FCP force-free activation energy.

A mix of *cis*-3FCP methyl ester and *trans*-3FCP methyl ester (20 mg) was dissolved in 1 mL *cis*-decalin in a pressured vessel and heated to 220 □. At each time point, the solution was allowed to cool down to room temperature. 0.1 mL aliquots were taken out and dissolved in 0.5 mL $CDCl_3$ followed by the addition of 30 μL benzoic acid solution (100

mg/mL in $CDCl_3$) as internal standard. ^{1}H NMR spectra were taken for each time point and the total amount of *cis*-3FCP *and trans*-3FCP was monitored as shown by Figure 6. Total amount of 3FCP was plotted against reaction time and fit with one phase exponential decay (Figure 7) to yield rate constant k_1 at 220□, which was further used to calculate $\Delta G_0^{\ddagger}$ at 220 □**.** Assuming the entropy contribution was negligible, the $\Delta G_0^{\ddagger}$ at RT was assumed to be the same with that at 220 □. Results are summarized in Table 9.

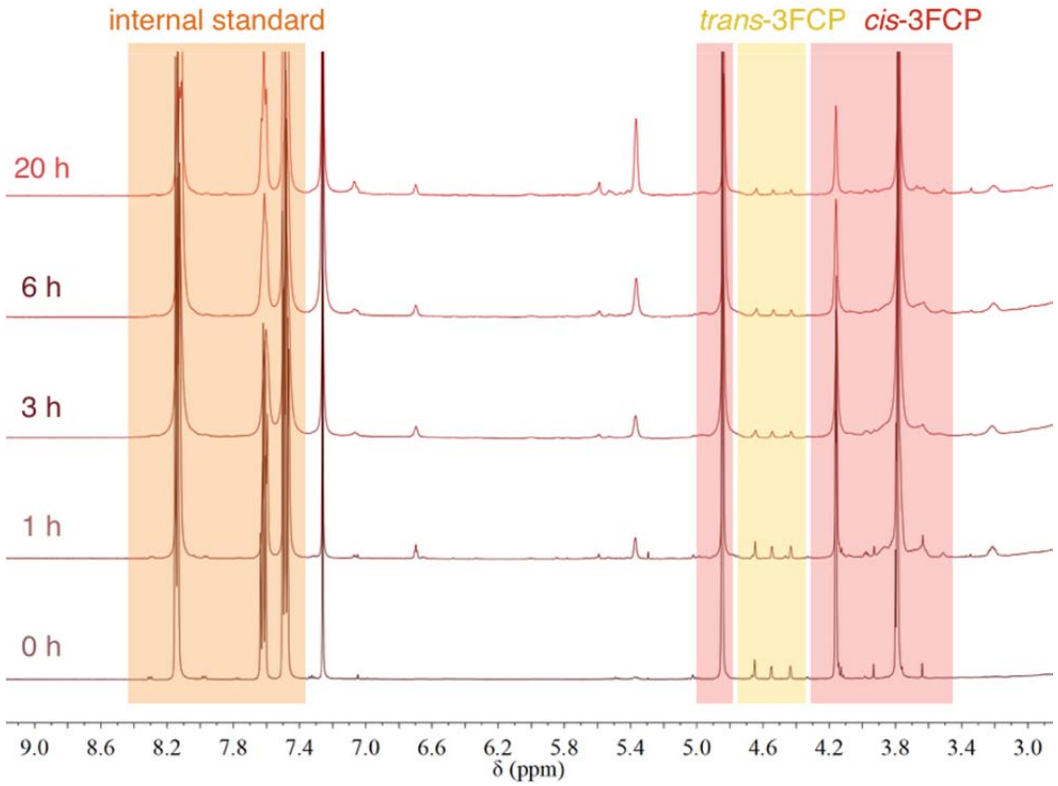

Figure 6. Overlay of ^{1}H NMR spectra of *cis*-, *trans*-3FCP methyl ester mixtures under heating at 220 □ for different times (normalized by the peak area of internal standard; δ=7.9-8.4 ppm).

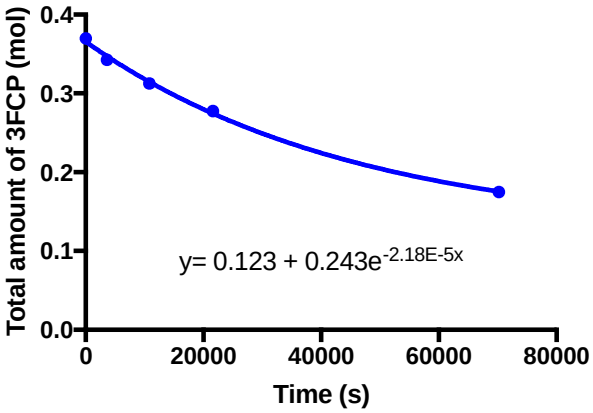

Figure 7. Total amount of *cis*-3FCP and *trans*-3FCP relative to internal standard change with time; fitted with one phase exponential decay y = a + b*$e^{-k1\ x}$ (a represents the equilibrium amount of 3FCP, b represents the decreased amount of 3FCP and k_1 represents the decomposition rate constant).

Table 9. Summary of force-free rate constant and activation energy of *cis*-3FCP

Entry	k_1 (s^{-1})	$\Delta G_0^{\ddagger}$ (kcal/mol)	k_0 (RT, s^{-1})
cis-3FCP	2.18E-5	39.9	2.95E-17
cis-5FCP	-	42.0[a]	1.01E-18

[a]Derived from the $\Delta G_0^{\ddagger}$ of *cis*-3FCP and the reported difference of ring strain between *cis*-3FCP and *cis*-5FCP according to Table 8.

7. Computational modeling

7.1 Polymer extension

CoGEF analysis was conducted following previous procedure using software SPARTAN' 10.[9] The end-end distance between two ends of the monomer (before and after activation) was constrained and the monomer structure deformed by increasing the end-end distance to the extent where the relative energy of the molecule is approximately 500 kJ/mol higher than that of equilibrium geometry. Then the constrained distance was released iteratively (~ 0.01 nm per step), and the relative energy of each step was determined. The analysis was conducted three times and the average value was used for the contour length change.

Detailed modeling procedure can be found in previously reported methods.[9]

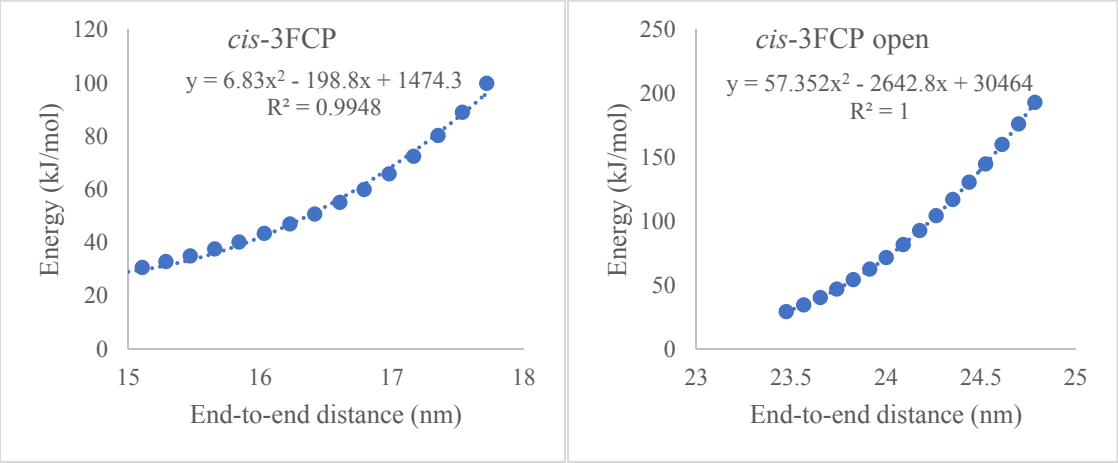

Figure 8. Example CoGEF analysis of *cis*-3FCP. The energies at each step are plotted vs. constraint distance (displacement) and fit with a quadratic (blue) to obtain the function of energy vs. displacement. The derivative of the fit provides a linear function of force vs. distance, which upon extrapolation to zero force provides the effective force-free end-to-end distance.

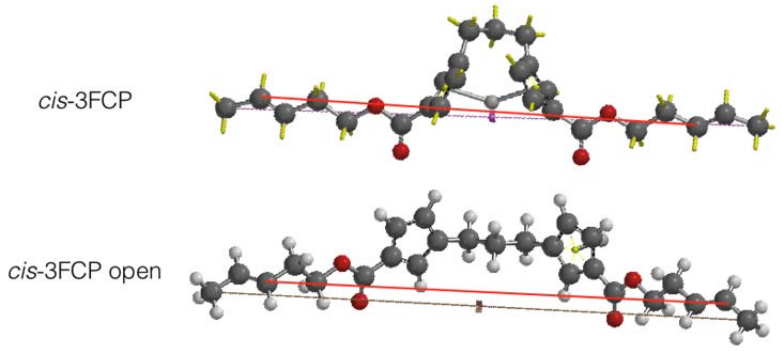

Figure 9. *Cis*-3FCP monomer structures with end-to-end distance indicated (red line).

Table 10. Force-free end-to-end distance of *cis*-[3]ferrocenophane

Entry	Try 1 (nm)	Try 2 (nm)	Try 3 (nm)	Average (nm)
L_1	1.46	1.44	1.45	1.45
L_2	2.30	2.31	2.31	2.31
L_2-L_1	-	-	-	0.86

Table 11. Force-free end-to-end distance of *trans*-[3]ferrocenophane

Entry	Try 1 (nm)	Try 2 (nm)	Try 3 (nm)	Average (nm)
L_1	1.64	1.64	1.65	1.64
L_2	2.25	2.25	2.30	2.27
L_2-L_1	-	-	-	0.63

Table 12. Force-free end-to-end distance of cis-[5]ferrocenophane

Entry	Try 1 (nm)	Try 2 (nm)	Try 3 (nm)	Average (nm)
$\mathbf{L_1}$	1.72	1.79	1.85	1.79
$\mathbf{L_2}$	2.74	2.75	2.73	2.74
$\mathbf{L_2\text{-}L_1}$	-	-	-	0.95

Table 13. Force-free end-to-end distance of epoxy-COD

Entry	All-*cis* (nm)	All-*trans* (nm)	Average (nm)
1	0.90	0.92	0.91

The ratio of polymer contour lengths, $L_{final}/L_{initial}$ are obtained from the following equation,

$$\frac{L_{final}}{L_{initial}} = \frac{(L_2 \times x) + (L_{epoxy-COD} \times (1-x))}{(L_1 \times x) + (L_{epoxy-COD} \times (1-x))}$$

where x denotes the molar fraction of FCP within the polymer as determined by ^{1}H-NMR spectroscopy, and L refers the end-to-end distance obtained from CoGEF calculations for the various monomers. A summary of simulation results is shown in Table 14 and Figure 10.

Table 14. Ratio of Polymer lengths before and after plateau

Entry	FCP molar ratio, x[a]	$L_{final}/L_{initial}$	
		SMFS[b]	modeling

***cis*-3FCP**	0.12	1.08 ± 0.06	1.10
	0.18	1.15 ± 0.02	1.15
***trans*-3FCP**	0.07	1.06 ± 0.02	1.05
	0.21	1.13 ± 0.09	1.18
***cis*-5FCP**	0.30	1.22 ± 0.02	1.24
	0.40	1.30 ± 0.05	1.32

[a]Molar ratio of FCPs in copolymer is determined from ^{1}H NMR integration. [b]Values are averages of the ratio of contour length after and before transition determined by fitting force curves to the freely jointed chain model.

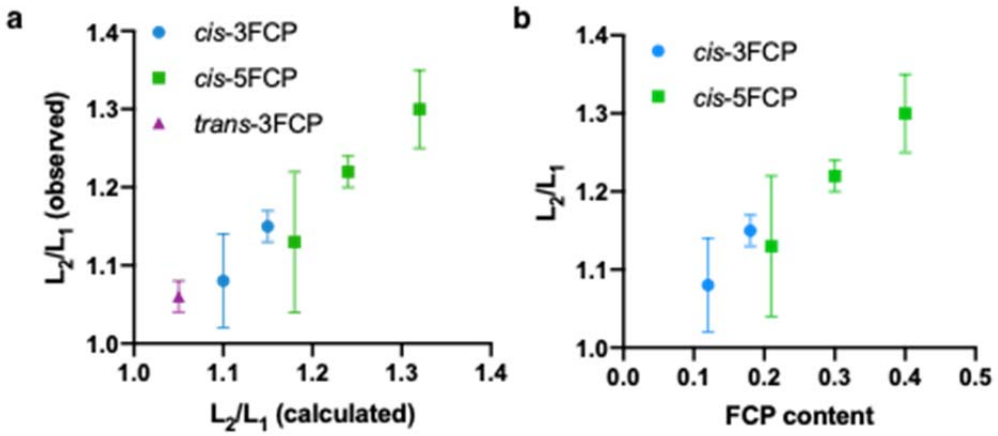

Figure 10. (a) Experimentally observed versus calculated polymer extension (L_2/L_1) for *cis*-3FCP (blue), *cis*-5FCP (green) and *trans*-3FCP (purple); (b) polymer extension (L_2/L_1) obtained from SMFS as a function of FCP content.

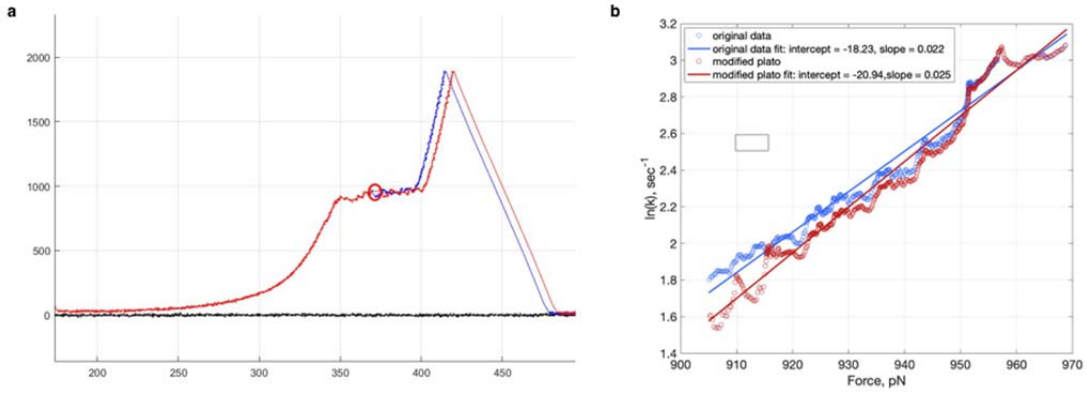

Figure 11. (a) A representative force-extension curve before (blue) and after (red) the manual insertion of a 5 nm "loop" release at the middle of the plateau. The introduction of the loop is used to estimate the potential impact of the rupture of one of a double tether on the extracted kinetics; (b) rate-force data before (blue circles) and after (red circles) the insertion. Blue and red line are the linear fits of these data points. Blue line: y = 0.022 x – 18.23; red line: y = 0.025 x – 20.94. The influence of such an event on calculated rates is < 10%.

7.2 Activation lengths

Transition states were taken as the geometry just before breaking (*cis*-3FCP: stretched distance = 14 Å; *trans*-3FCP: stretched distance = 11.5 Å; *cis*-5FCP: stretched distance = 14 Å). All carbon atoms on the Cp ring of the ground states were frozen and four carbon atoms on the Cp ring (C_2, C_3, C_4, C_5) of the transition states were frozen during CoGEF analysis to account for the distortion of Cp ring during stretching. CoGEF simulation on the ground states and transition states were performed as described in section 3. The difference between the force-free end-to-end distance of transition state L_{TS} and ground states L_{GS} yields $\Delta x^{\ddagger}$. The obtained $\Delta x^{\ddagger}$ was then used to estimate $\Delta G^{\ddagger}$ using the cusp model. The results were summarized as below.

Table 15. Summary of force-free activation length obtained by CoGEF modeling and force-free rate constants obtained by fitting with a cusp model

Entry	L_{GS} (nm)	L_{TS} (nm)	$\Delta x^{\ddagger}$ (nm)	$\Delta G^{\ddagger}$ (cusp, kcal/mol)	k_0 (cusp, s^{-1})
cis-3FCP	13.9±0.11	16.9±0.04	3.0±0.12	42-43	1.9E-19 - 1.0E-18
trans-3FCP	14.9±0.17	17.0±0.02	2.2±0.17	41-42	1.0E-18 - 5.5E-18
cis-5FCP	14.2±0.02	17.1±0.15	2.9±0.15	45-46	1.2E-21 - 6.4E-21

7.3 CoGEF of ferrocenophane dissociation

The stretched structure evolution of ferrocene was explored with Gaussian 09. 1,1'-ferrocenedicarboxylic allyl diester was selected as the model compound for calculation because it well matches with the structure unit in the polymer chain for this study. Very recently, Li et al. used DFT calculation to simulate the elongation process from external force on ferrocene, and the simulation results agreed with experiment results.6 Based on this benchmark calculation study, we utilized the same DFT calculation method: UB97D function was employed to describe the system, along with the def2-svp basis sets for C, H, and O atoms and the more extensive def2-tzvp basis set for Fe. Solvent effects (THF) were included using the SMD implicit solvation model. CoGEF (constrained geometry simulates external force) method proposed by Beyer et al was used to model the contour length.7 Briefly, the end-to-end distance of the model compound was fixed to specific values to mimic the imposed force, meanwhile all other geometric coordinates were allowed to fully relax. Then equilibrium geometry and energy were determined at iteratively increased end-to-end distance until the good separation between molecular segments after chain scission. The relationship of force and elongated distance can be obtained from a curve of the 1st derivate of energy to distance. The fully relax model compound energy was normalized to 0 kJ/mol.

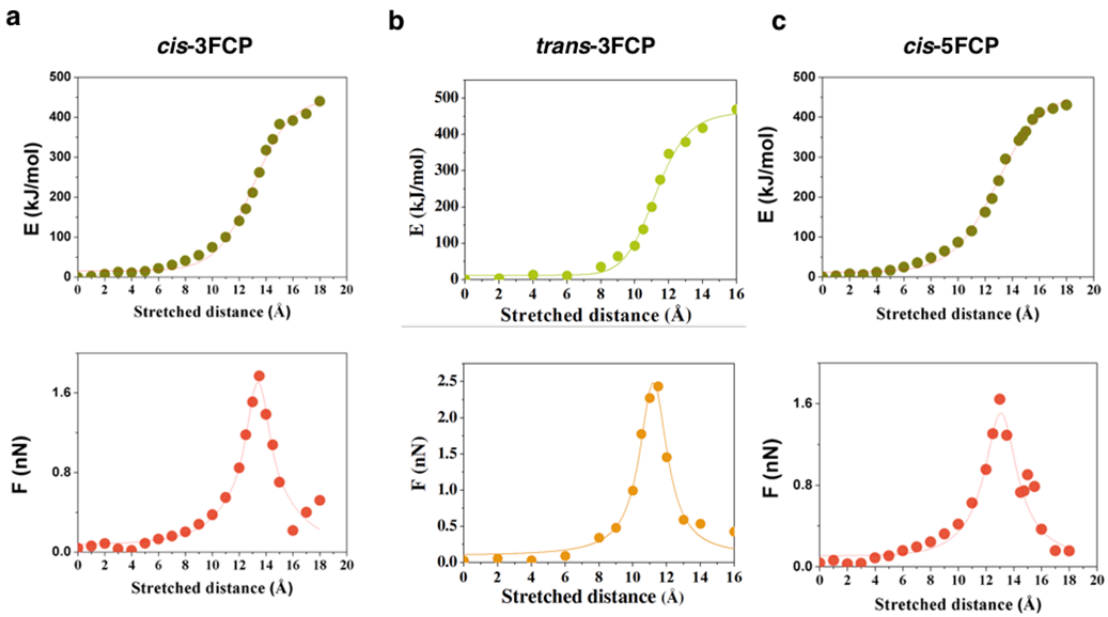

Figure 12. CoGEF potential and force as a function of stretched distance for *cis*-3FCP (a), *trans*-3FCP (b) and *cis*-5FCP (c) model compounds. The stretched distance defined as 0 Å when no stress is applied.

The dissociation energy of *cis*-3FCP, *trans*-3FCP and *cis*-5FCP can be calculated from the energy at breaking point (14.5 Å for *cis*-3FCP, 12 Å for *trans*-3FCP and 14.5 Å for *cis*-5FCP) and summarized in Table 16.

Table 16. Summary of the dissociation energy of ferrocenophanes.

Compound	Dissociation energy (kcal/mol)
cis-3FCP	80
trans-3FCP	83
cis-5FCP	82

7.4 CoGEF of alternative pathways

To further examine the effect of shearing versus peeling on ferrocene dissociation, we fixed the side chain angle of a ferrocene monomer to 0° during stretching so that two Cp ligands were aligned in an eclipsed geometry, which will effectively drive the ferrocene to go down the peeling pathway. After the ferrocene dissociates, the fix applied on the side chains was removed. Similarly, CoGEF calculations were performed to obtain the equilibrium structure at each step as end-to-end distance is increased. The geometry evolutions were shown in Figure 11b. In contrast, when no fix was added on side chains, stretching would result in the rotation of Cp rings and dissociate through a shearing pathway as shown in Figure 11a.

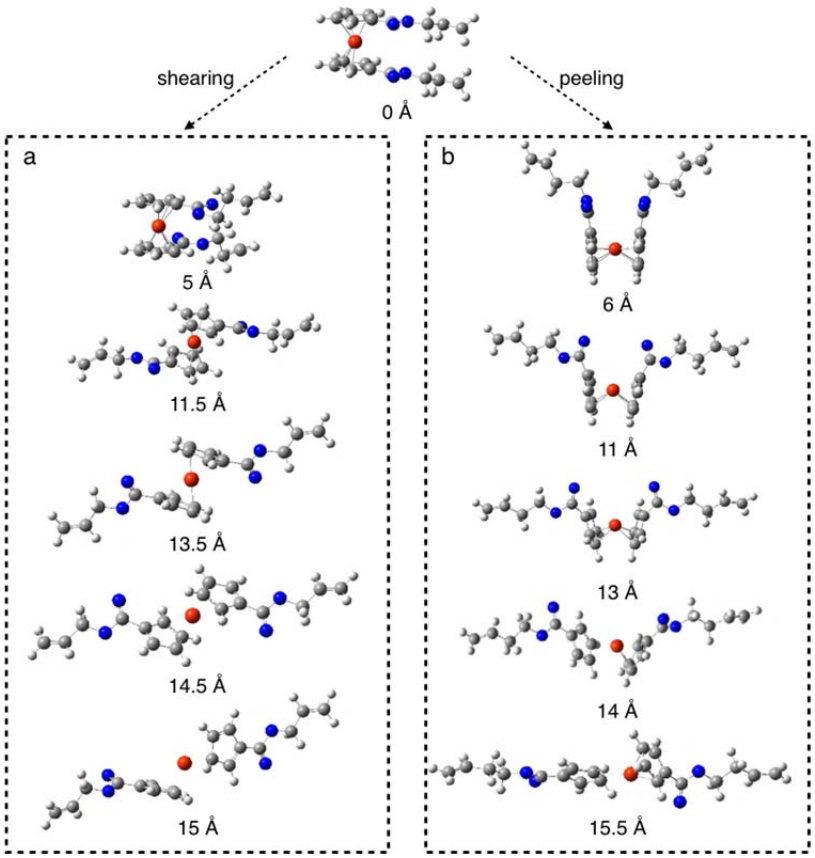

Figure 13. Structural evolution of ferrocene that goes down a shearing pathway (a) without restriction on the side chain angles, and peeling pathway (b) by fixing the side

chain angles close to 0°.

We then compare the CoGEF energy of the two pathways. As shown in Figure 12, the maximum force on the potential energy surface, which suggests an upper limit for ferrocene dissociation, is much smaller for peeling (1.1 nN, Figure 12a) than shearing (3.1 nN, Figure 12b). The dissociation energy (an upper limit of activation energy) can be calculated from the energy at breaking point (14 Å for peeling pathway and 14.5 Å for shearing pathway) and summarized in Table 17. It is shown that the dissociation energy through the peeling pathway is only 65 kcal/mol, which is substantially lower than the shearing pathway (87 kcal/mol). These results suggest that a change in dissociation mechanism from shearing to peeling substantially lowers the force-coupled activation energy, thus leading to enhanced mechanochemical reactivity and is consistent with our observations from sonochemistry[5] and SMFS experiments.

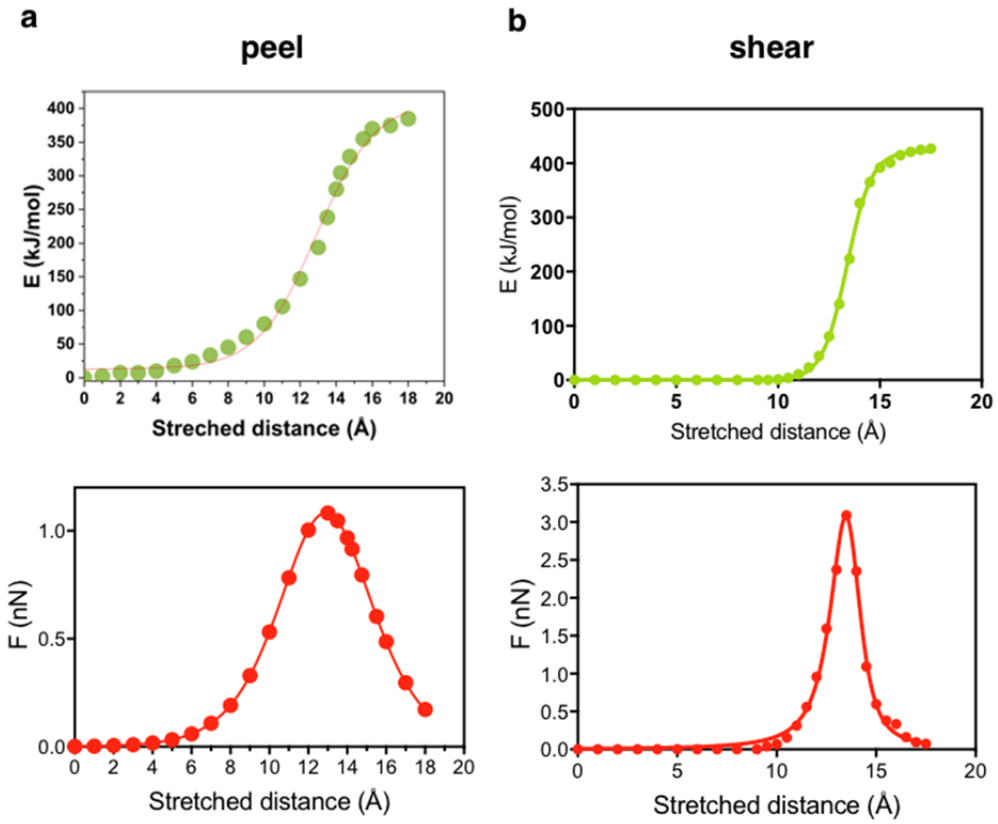

Figure 14. CoGEF potential and force as a function of stretched distance for ferrocene model compound that undergoes peeling (a) and shearing (b) pathways. The stretched distance defined as 0 Å when no stress is applied.

Table 17. Summary of ferrocene dissociation energy under different pathways

Compound	Pathway	Energy penalty (kcal/mol)	Maximum Force (nN)
Ferrocene	Peel	65	1.1
Ferrocene	Shear	87	3.0

7.5 Summary of displacement projection of ferrocene derivatives

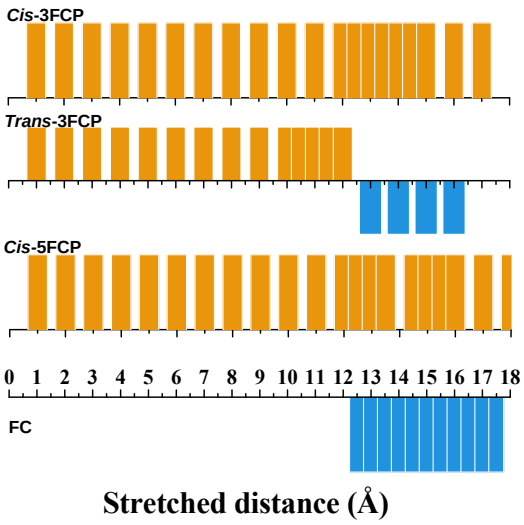

Figure 15. Summary of displacement projection for different ferrocenyl structures during stretching. Orange bar presents "+" projection toward the right side of the center of the bottom Cp, while blue bar represents "-" projection toward the left side.

7.6 Measurements of angle α and β

The measurement of the dihedral angles of the two planes (α) were done in Mercury. The equilibrium geometry is obtained from DFT optimization and imported into Mercury. Two planes were created using the 5 carbon atoms of the cyclopentadiene ring and then the dihedral angles of the two planes (α) were read automatically.

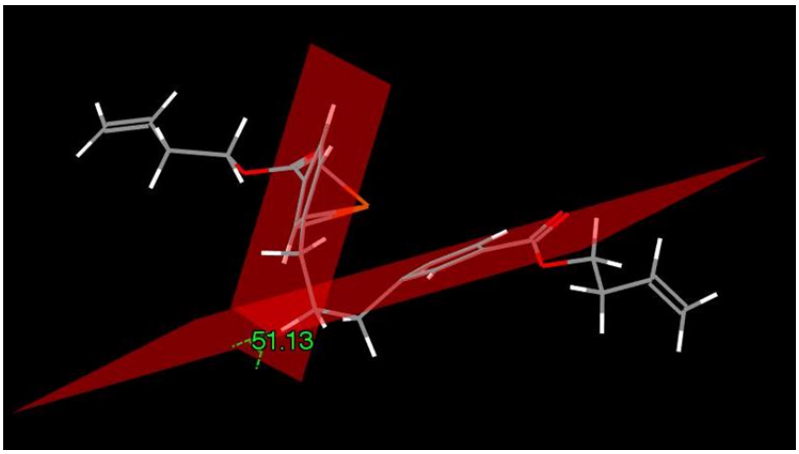

Figure 16. Example of measurement of Cp plane-plane dihedral angles for *trans*-3FCP at breaking point (displacement = 12 Å).

The measurement of the dihedral angle between side chains (β) were done in Gaussian 09. The equilibrium structure is obtained from DFT optimization. 4 atoms from the two side chains (highlighted in Figure 14) were selected following this order: 21, 2, 7, 18. The dihedral angles were read automatically from the software.

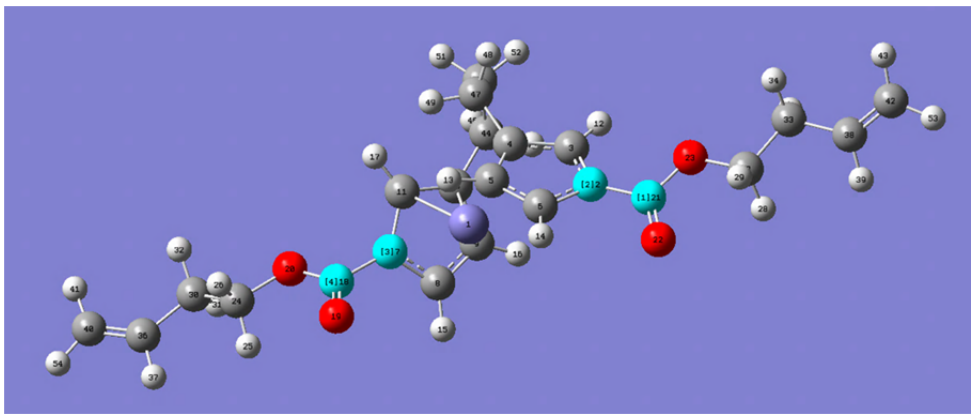

Figure 17. Example of measurement of side chain dihedral angles for *trans*-3FCP at breaking point (displacement = 12 Å).

7.7 Effect of the *ansa* bridge

Comparing the dissociation energy between *cis*-3FCP and un-bridged ferrocene, both of which undergoes the peeling pathway, we find that interestingly, the dissociation energy for *cis*-3FCP (80 kcal/mol) is higher than ferrocene (65 kcal/mol) despite their very similar thermal stabilities. This can probably be attributed to the increased energy due to the distortion of bond angles between the *ansa*-bridge and Cp ligands when being stretched. Two pieces of evidence could support this: The Cp-Cp dihedral angle change is smaller for *cis*-3FCP compared to ferrocene under the same strain (Figure 15); H-H distance on C_1 and $C_{1'}$ for ferrocene decreases with stretching while the C_6-C_8 distance of *cis*-3FCP remains almost constant (Figure 16).

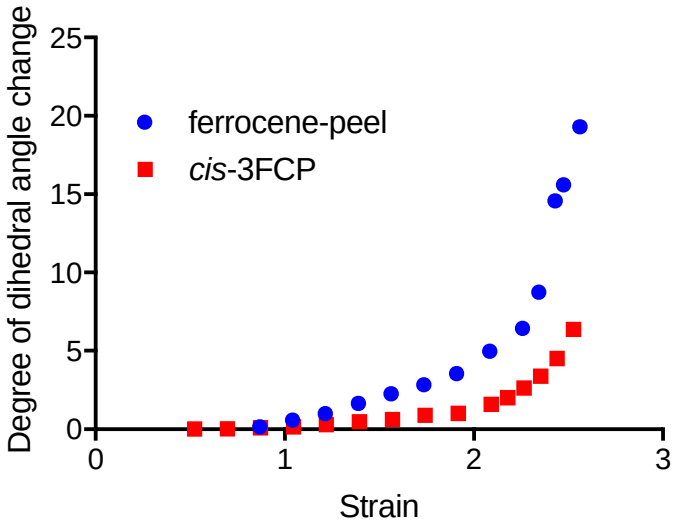

Figure 18. Degree of dihedral angle change (defined as Cp-Cp dihedral angle change over initial angle) under different strain (defined as end-to-end distance change over initial distance).

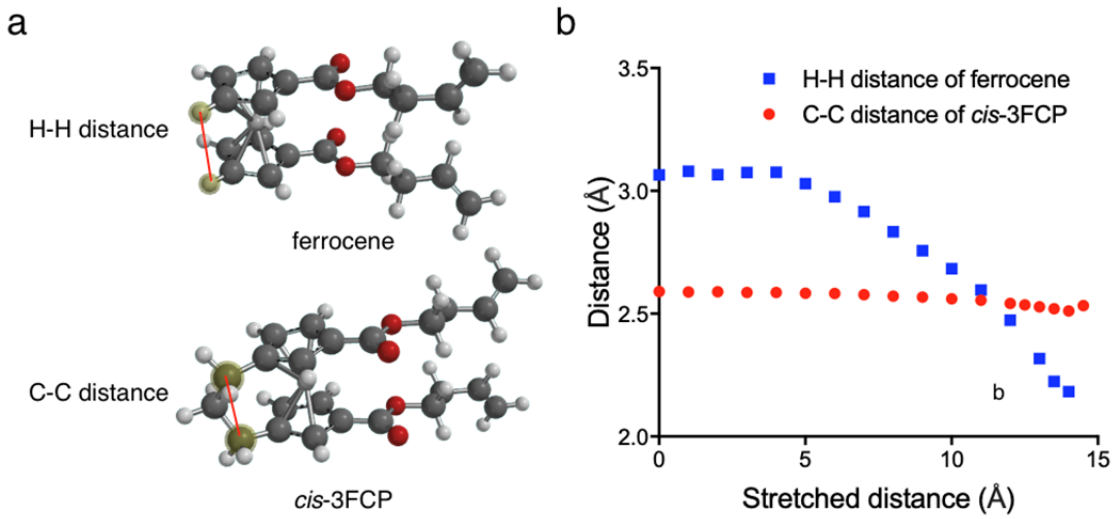

Figure 19. (a) Illustration of the measurement of C-C distance for *cis*-3FCP and H-H distance for ferrocene; (b) Distance change with stretched distance.

8. Bulk mechanochromism

8.1 Drop test

A *cis*-3FCP/ferrocene embedded silicone plug is placed inside a 20 mm diameter hardened steel dry compression die. An iron bar weighing 6.38 kg is held 10 cm above the compression die. Then the weight is released so that it drops freely to strike the die.

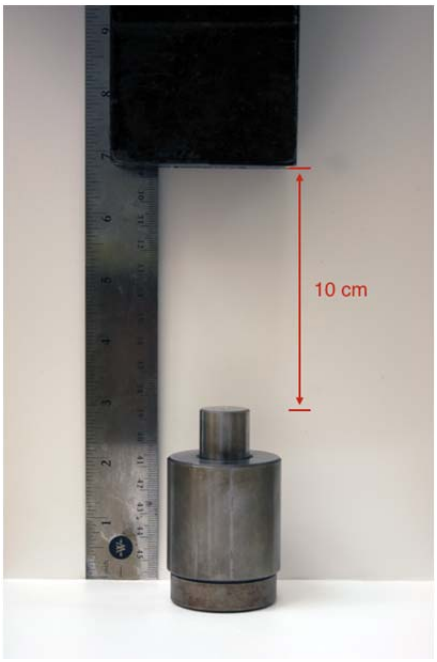

Figure 20. Drop test illustration. The distance between the compression die and the weight is 10 cm.

8.2 Quantification of mechanophore activation after drop test

Two cylindrical silicone samples (0.25 inch in diameter) were prepared according to the procedures described in section 1.5 and cut into disks with 1-3 mm in thickness. The UV-Vis spectra of the samples before and after the drop test were collected using a CCD array UV-Vis spectrometer.

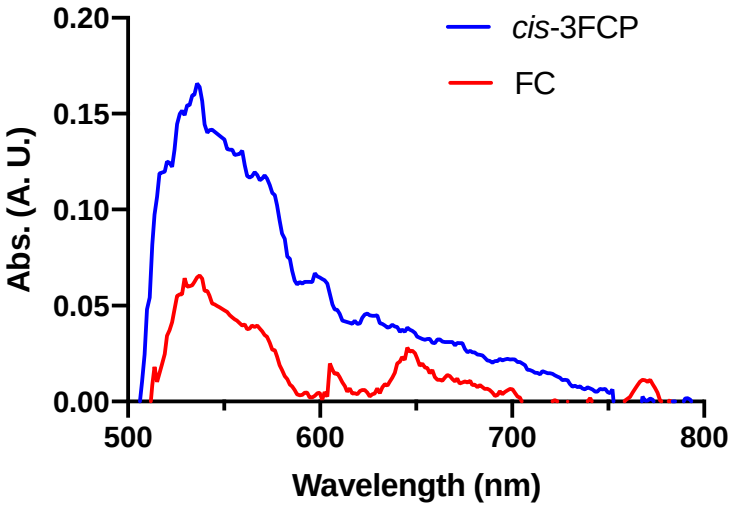

Figure 21. UV-Vis spectra of silicone samples embedded with *cis*-3FCP and FC respectively after the drop test. Absorbance before the drop test was subtracted and the remaining signals were normalized to 1mm cell path length. The peak at ~530 nm corresponds to the mechanically formed Fe^{2+}-phenanthroline complex.

The activation ratio of cis-3FCP and FC could be calculated taken the peak intensity at ~530 nm from Figure 11 and the molar absorptivity (ε) of Fe^{2+}-phenanthroline complex.[17]

Total concentration of *cis*-3FCP: c(*cis*-3FCP) = 5/422 = 1.2E-2 mol/L

$c(Fe^{2+})$ =Abs/(ε*b) = 0.16/(1.1E4*0.1) = 1.4E-4 mol/L

Activation ratio (*cis*-3FCP) = 1.4E-4/1.2E-2 = 1.2%

Total concentration of FC: c(FC) = 5/382 = 1.3E-2 mol/L

$c(Fe^{2+})$ =Abs/(ε*b) = 0.06/(1.1E4*0.1) = 5.4E-5 mol/L

Activation ratio (FC) = 5.4E-5/1.3E-2 = 0.4%

8.3 Split Hopkinson pressure bar test

A polycarbonate split Hopkinson bar is used to generate repeatable, measured impact loading on both the *cis*-3FCP and FC specimens. The measured average peak stress and strain values are show in Table 18 to verify that all specimens were subjected to similar loading. As shown in Figure 20, *cis*-3FCP shows a more prominent color change compared to ferrocene.

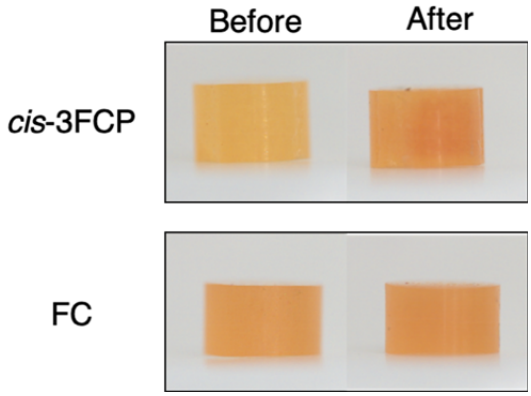

Figure 22. Representative photos of *cis*-3FCP (top) and FC (bottom) embedded silicone specimen that were before (left) and after (right) a split Hopkinson pressure bar test with similar experimental parameters.

Table 18. Average peak stress and strain of *cis*-3FCP and FC embedded silicone specimen for the split Hopkinson pressure bar test

Entry	Peak stress (MPa)	Peak strain
cis-3FCP	19.46±3.08	0.60±0.10
FC	18.44±1.98	0.57±0.07

8.4 Uniaxial tension

A thin film (~0.5 mm in thickness) was obtained by pouring the prepolymer mixture onto a PTFE surface. Once cured, the film was further cut into stripes for testing. Tensile elongation results in a color change within the gauge region of a hand-stretched sample as shown below.

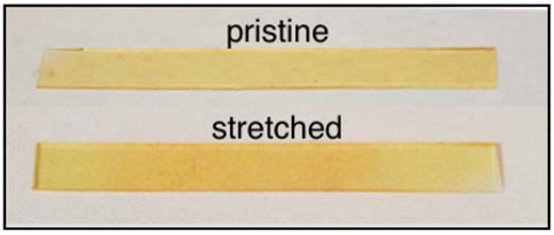

Figure 23. Uniaxial stretching (~100% strain) of a *cis*-3FCP containing PDMS film.

The UV-vis spectrum of the stretched and pristine thin film as shown is Figure 13 was measured and shown as below. A characteristic peak at ~ 520 nm, which is attributed to the formation of Fe^{2+}-phenanthroline complex, appears for the stretched sample.

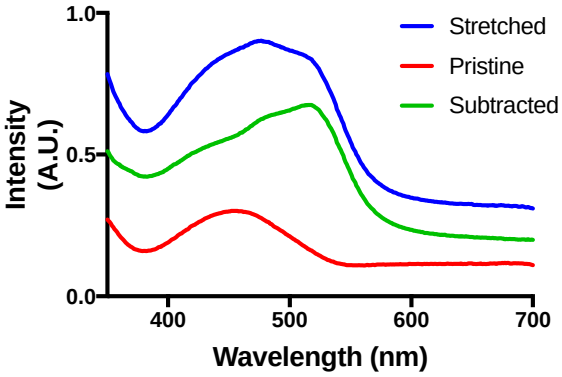

Figure 24. Normalized UV-vis spectrum of silicone elastomer embedded with *cis*-3FCP before and after stretching

8.5 Use of TPTZ as a trapping ligand

To demonstrate that different color change can be achieved by simply using a different exogenous ligand, a solution of TPTZ was used to swell the cured silicone plug. The solvent was subsequently removed by evaporation, leaving TPTZ in the intact plug. Upon a hammer strike, the specimen developed a dark brownish color consistent with the formation of the expected blue-purple iron complex within the yellow material, as shown below.

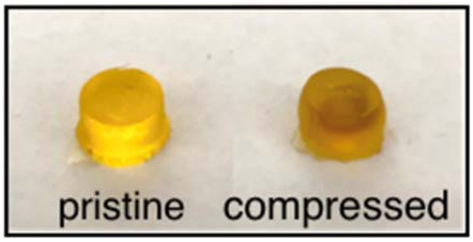

Figure 25. Pristine (left) and compressed (right) *cis*-3FCP embedded silicone plug that contains TPTZ as an exogenous ligand.

9. Cross-linking

9.1 Sonication of 9

A 2 mg/mL solution of polymer 9 was sonicated for 30 min. When the solvent was removed, the remaining polymer is not soluble in common solvents. $CDCl_3$ was added to the crosslinked polymer to extract the soluble part and ^1H NMR is shown below. No peaks for the activated ferrocene were observed.

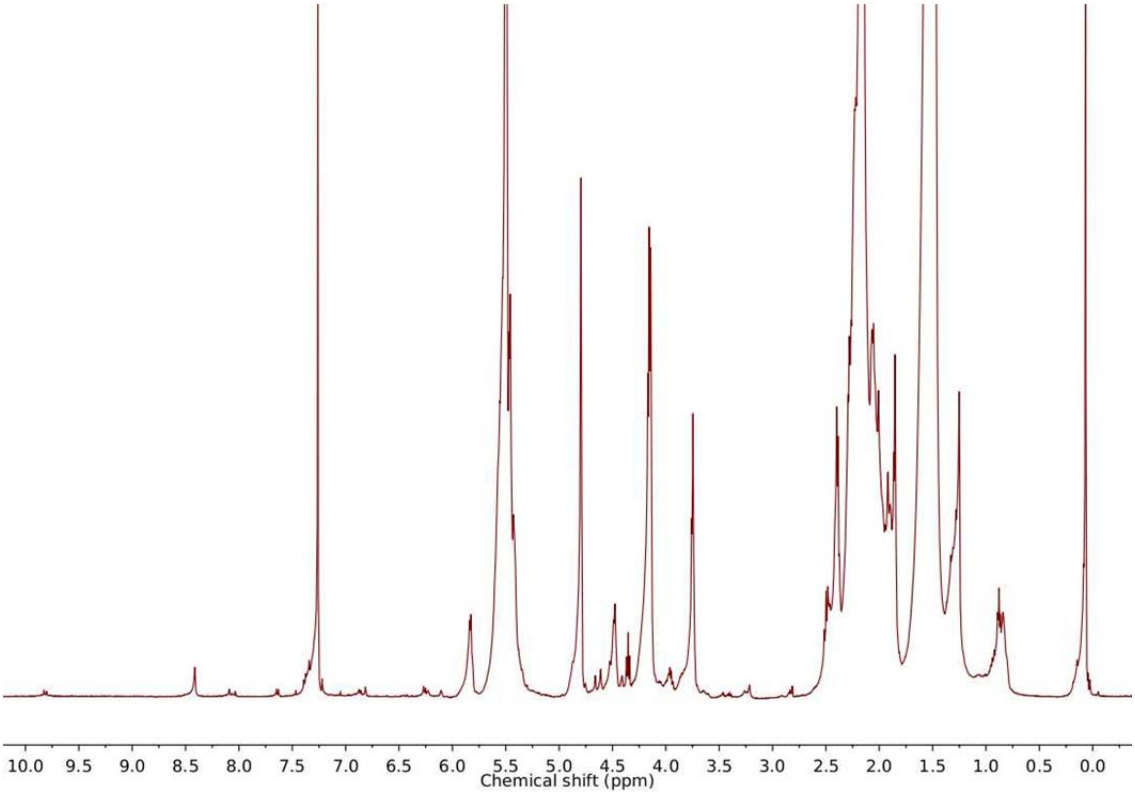

Figure 26. ^1H NMR spectrum for the soluble part of 9 after 30 min. Peak for Cp (δ=6.6, 6.7, 7.4 ppm) is not observed.

9.2 Sonication of 11 with pyrenyl-maleimide

26 mg **11** and 125 mg pyrenyl-maleimide (3 equivalence of total amount of *cis*-[3]ferrocenophane) were dissolved and sonicated in 13 mL THF. Aliquot was taken

out after 2 h. Solvent was removed and washed with MeOH for 2 times. The polymer is completely soluble in THF (Figure 25) and injected directly into GPC. The proposed DA reaction process is shown in Scheme 1. The UV signals collected were shown in Figure 26 and 27.

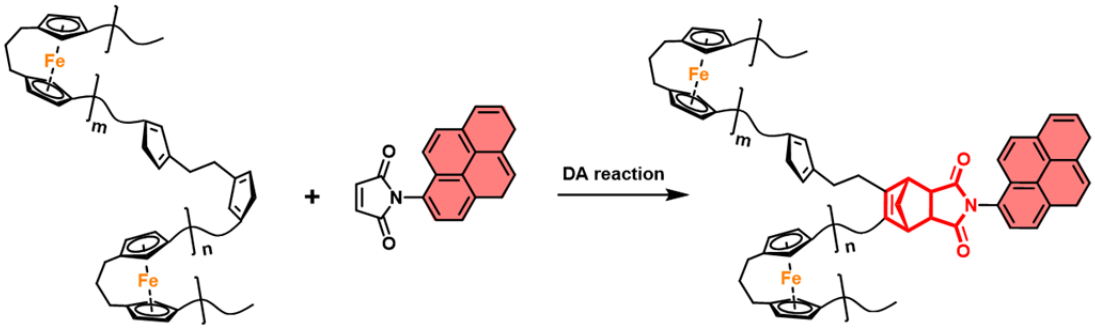

Scheme 1. DA mechanism of Cp with pyrenyl-maleimide.

Figure 27. Photos of polymer solution with pyrenyl-maleimide before (left) and after 30 min sonication (right).

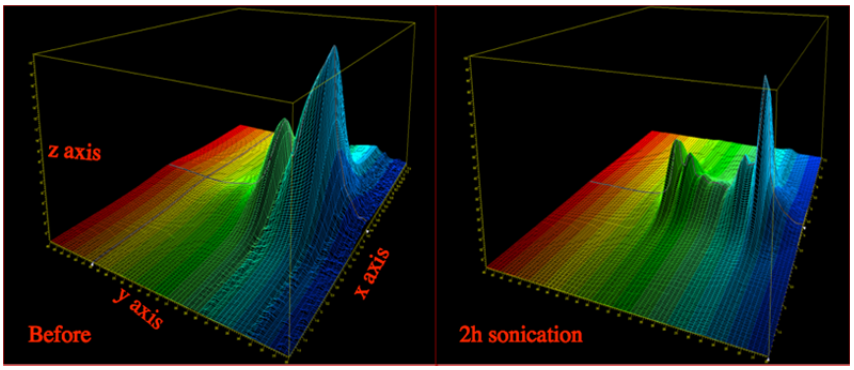

Figure 28. UV signals of **11** before and after 2h sonication in the presence of pyrenyl-maleimide. X axis represents retention time (11-17 min), Y axis represents wavelength (200-460 nm), Z axis represents intensity.

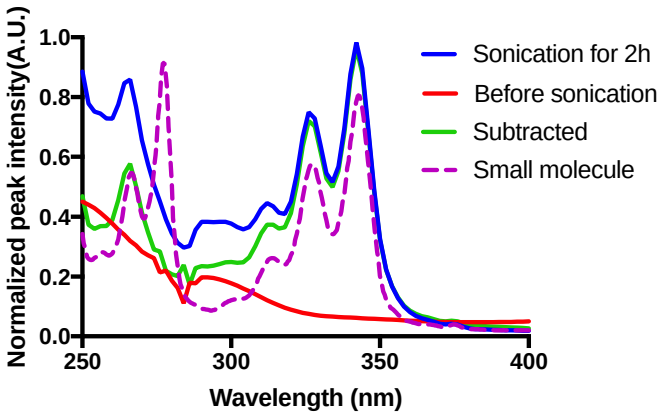

Figure 29. Absorbance spectrum of **11** in the presence of pyrenyl-maleimide (10 mg/mL) at retention time = 14.4 min.

10. NMR spectra

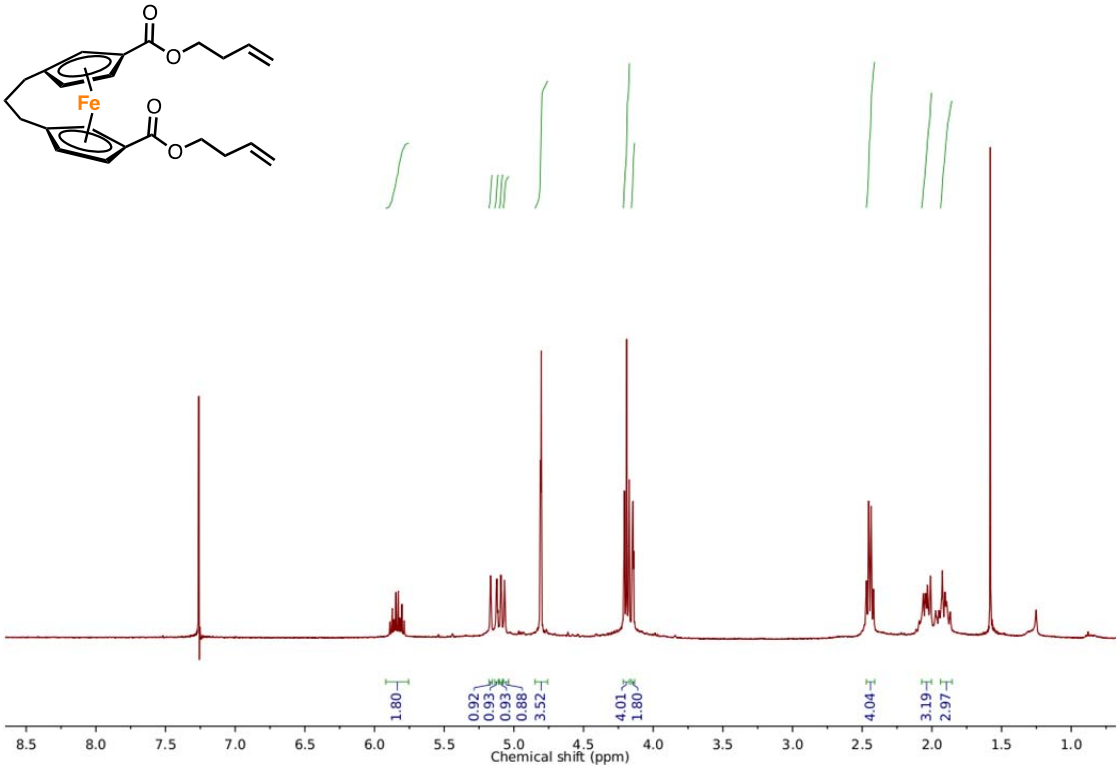

Figure 30. ^{1}H NMR spectrum of **1** in $CDCl_3$.

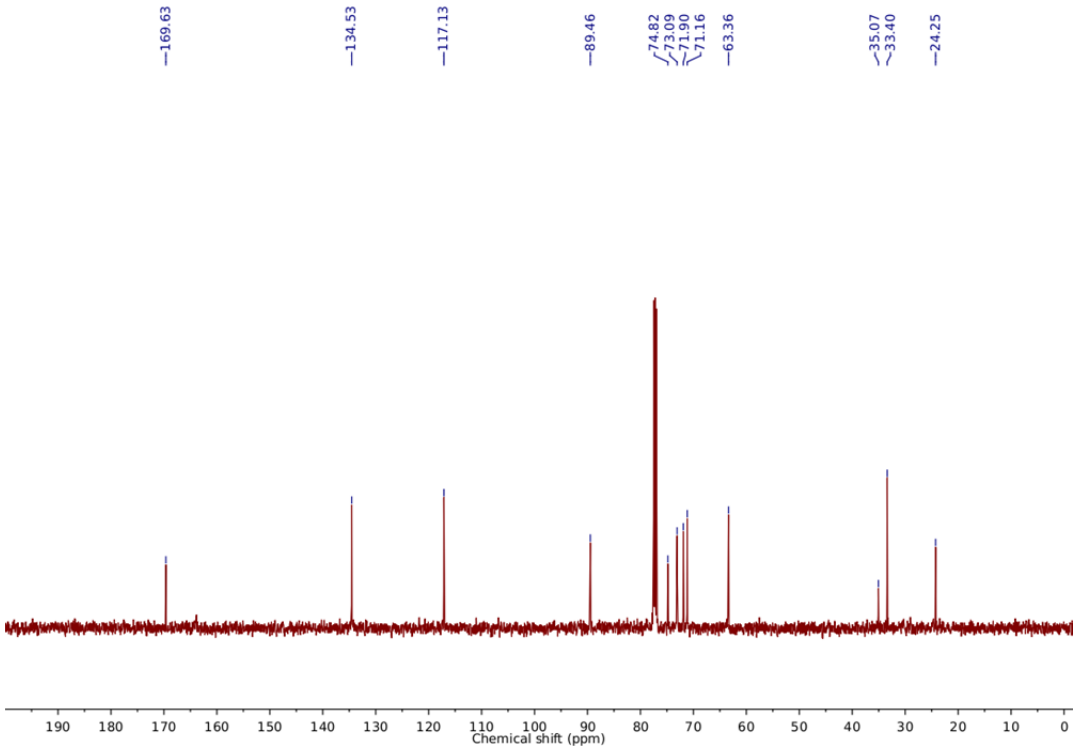

Figure 31. ^{13}C NMR spectrum of **1** in $CDCl_3$.

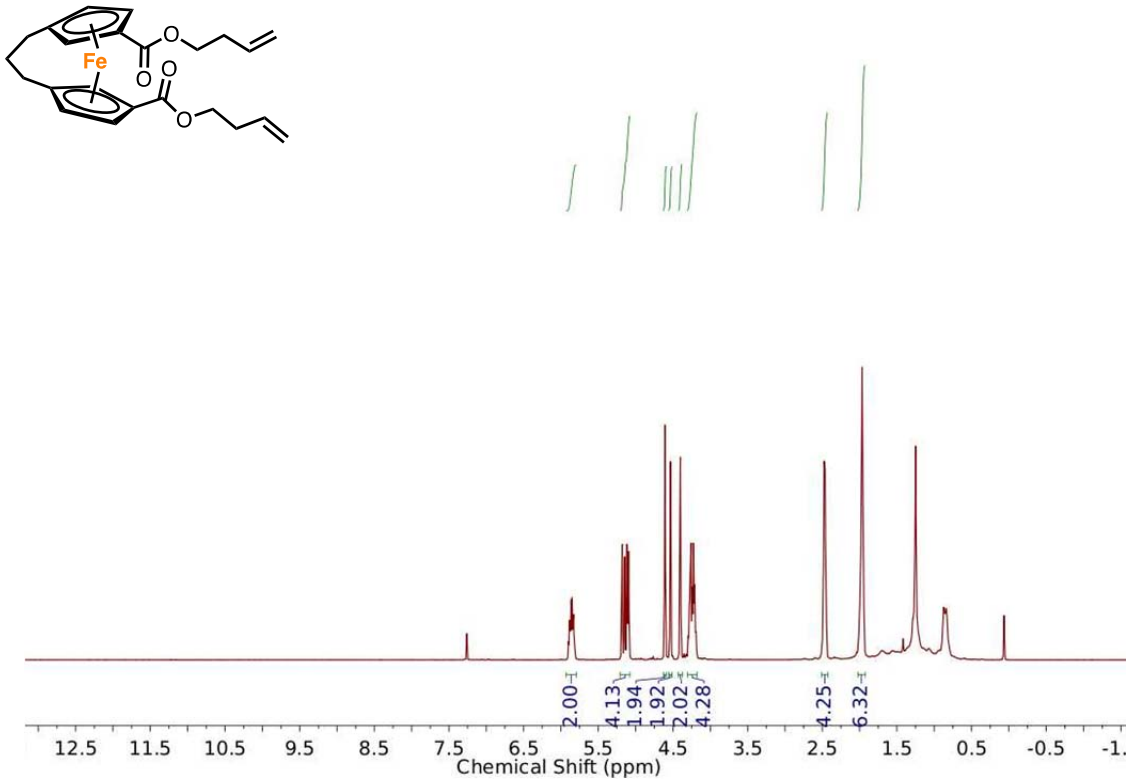

Figure 32. ^{1}H NMR spectrum of **2** in $CDCl_3$.

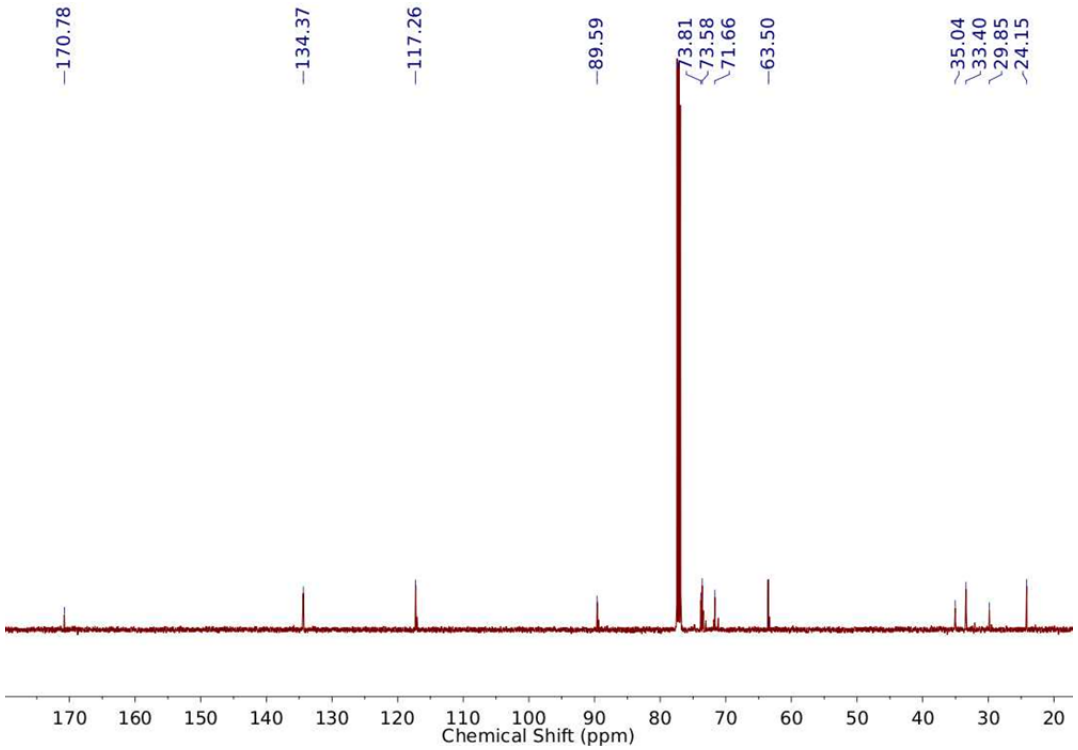

Figure 33. ^{13}C NMR spectrum of **2** in $CDCl_3$.

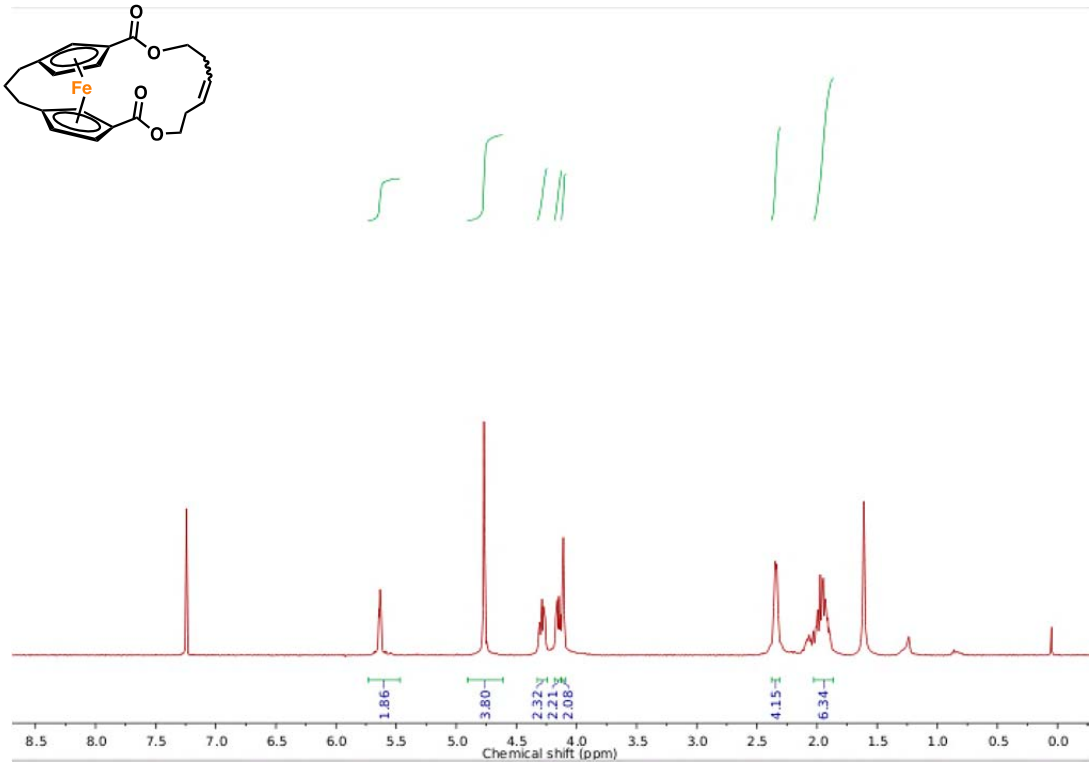

Figure 34. ^{1}H NMR spectrum of **3** in $CDCl_3$.

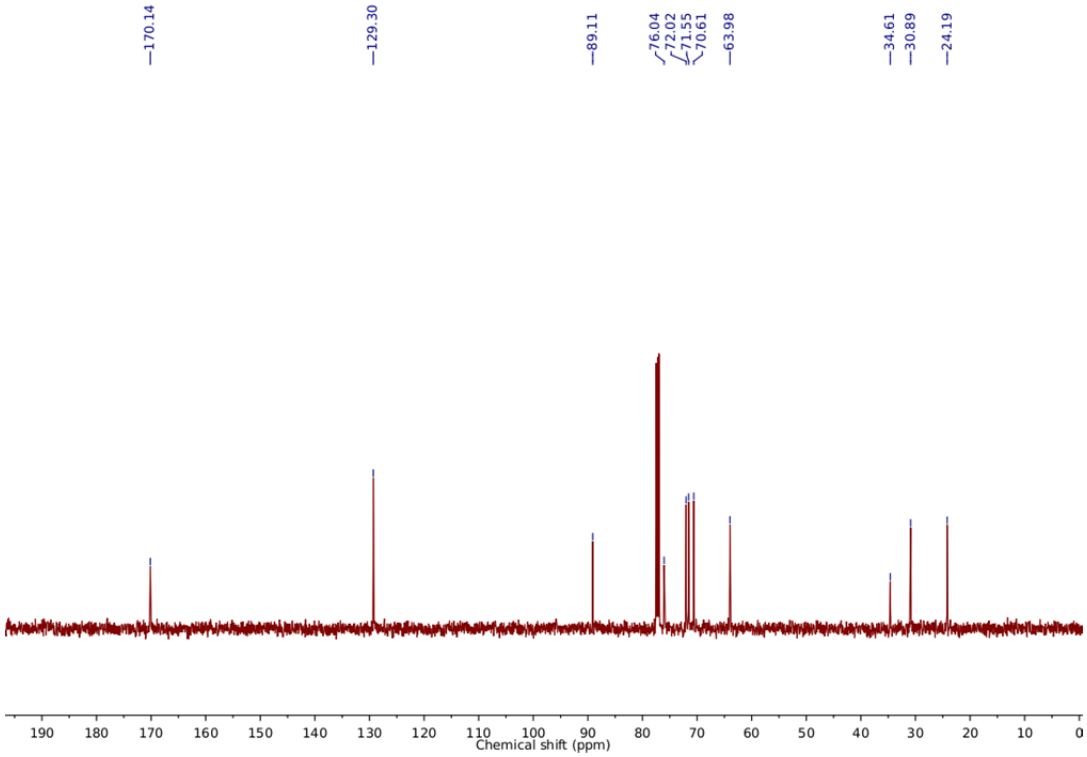

Figure 35. ^{13}C NMR spectrum of **3** in $CDCl_3$.

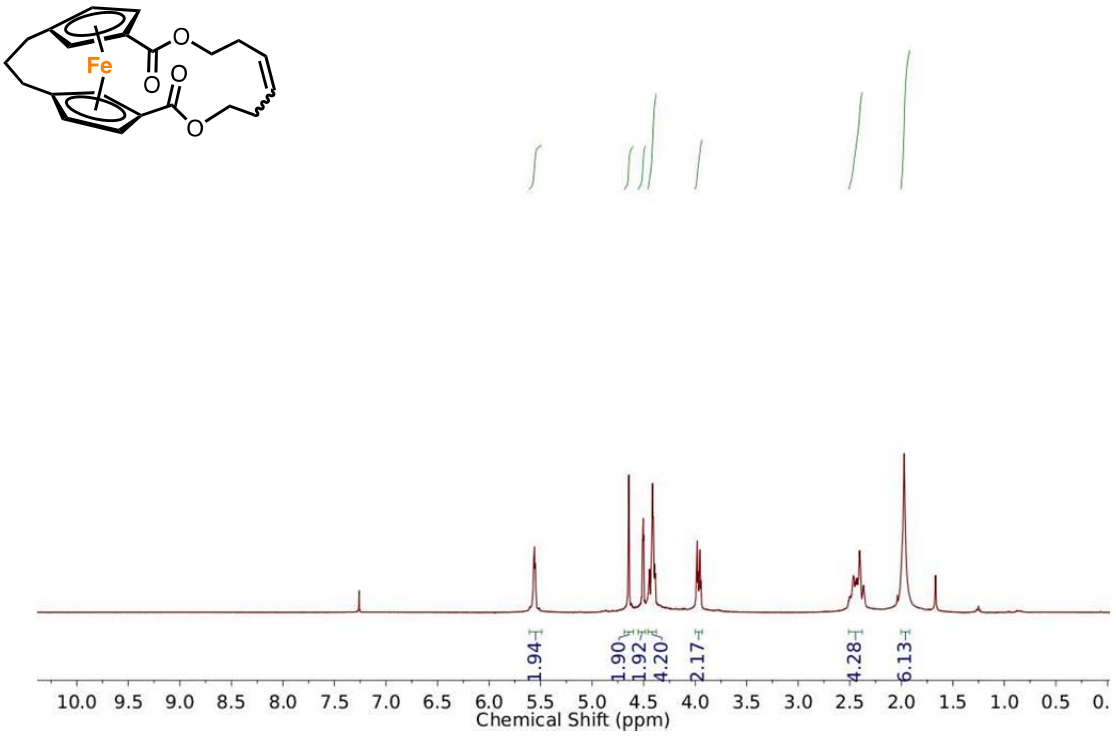

Figure 36. ^{1}H NMR spectrum of **4** in $CDCl_3$.

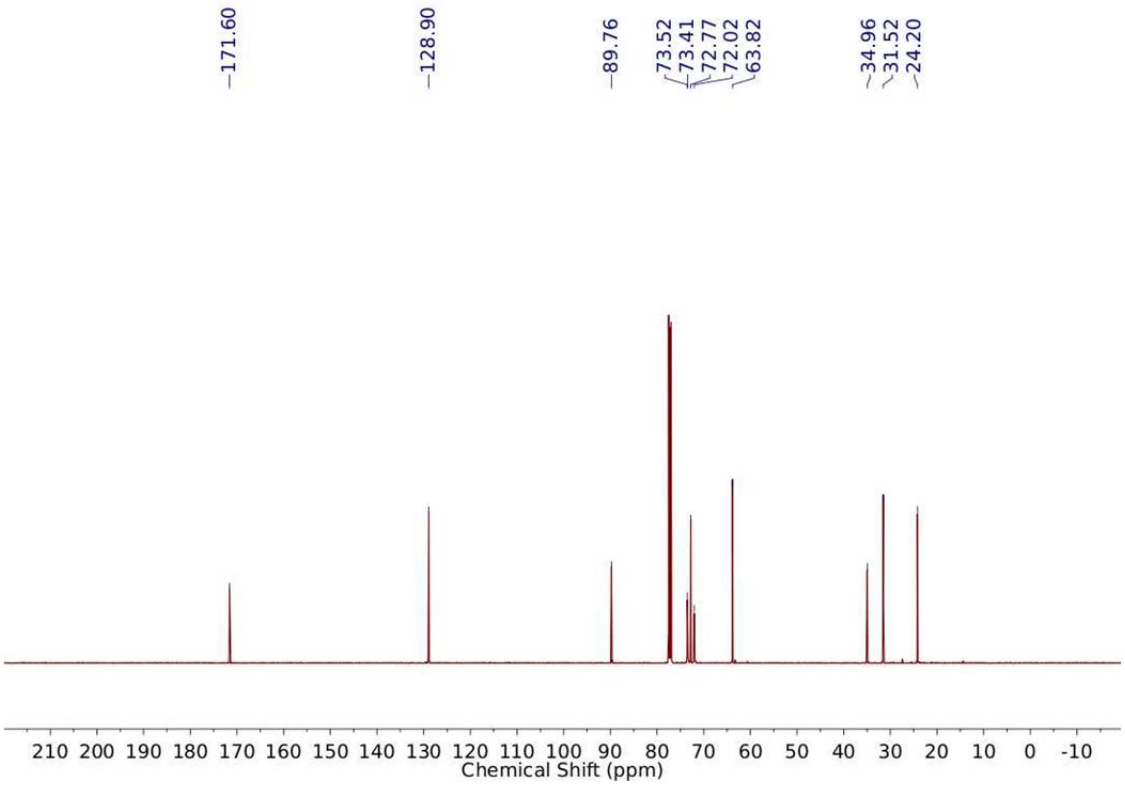

Figure 37. ^{13}C NMR spectrum of **4** in $CDCl_3$.

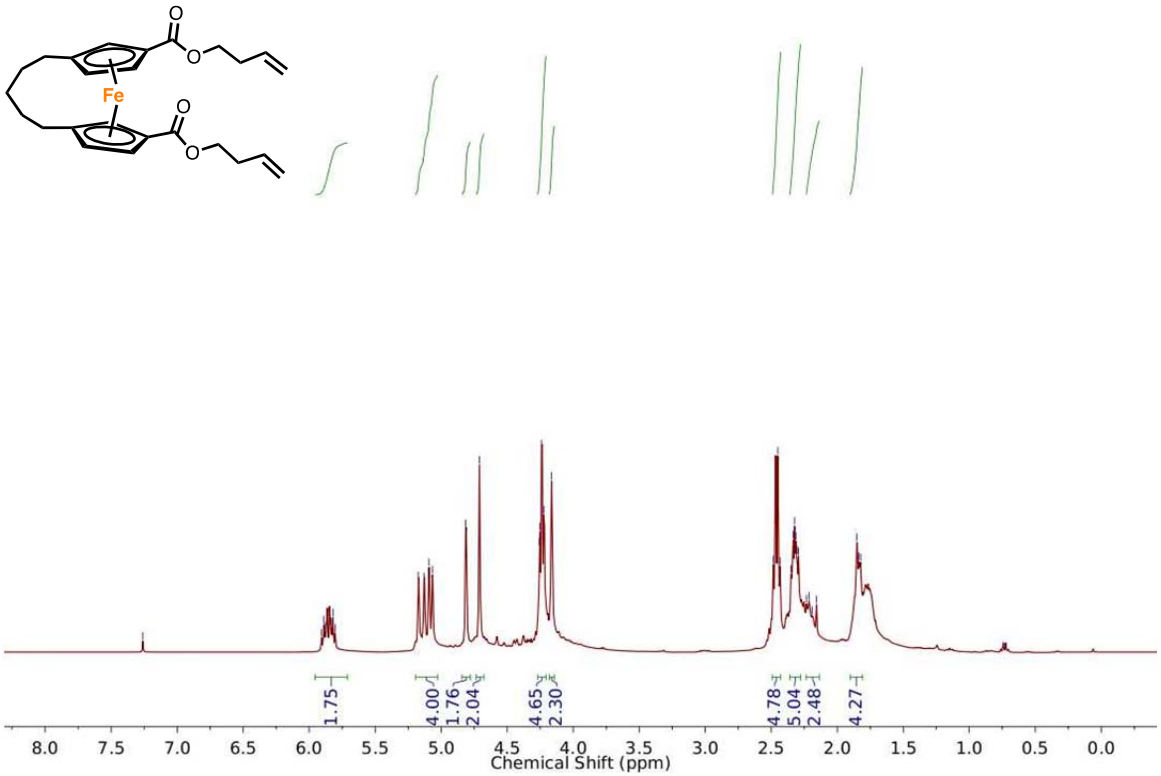

Figure 38. ^{1}H NMR spectrum of **5** in $CDCl_3$.

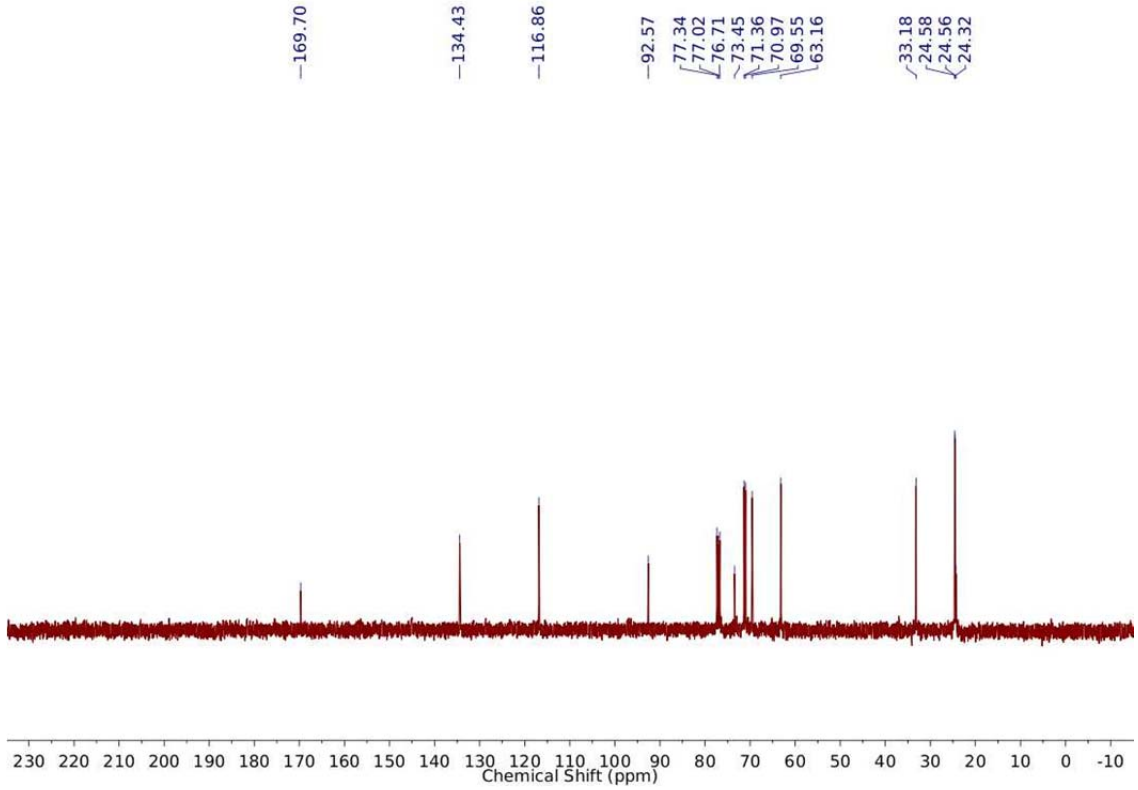

Figure 39. ^{13}C NMR spectrum of **5** in $CDCl_3$.

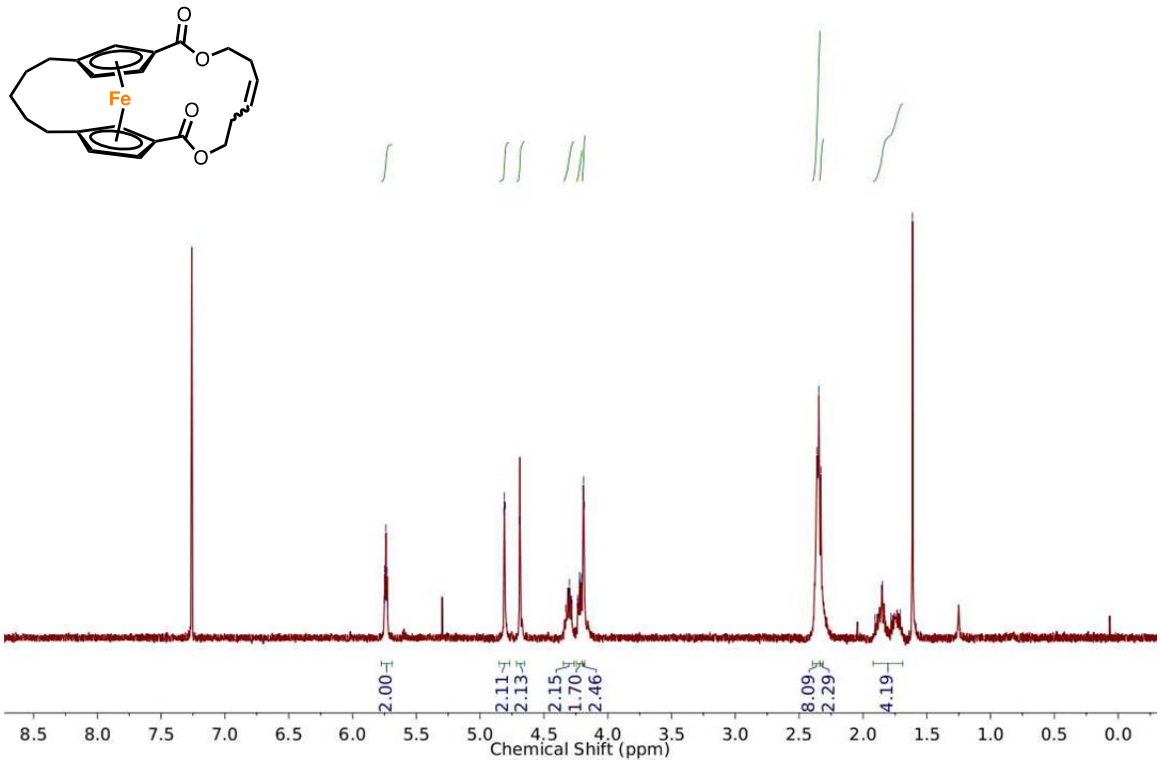

Figure 40. ^{1}H NMR spectrum of **6** in $CDCl_3$.

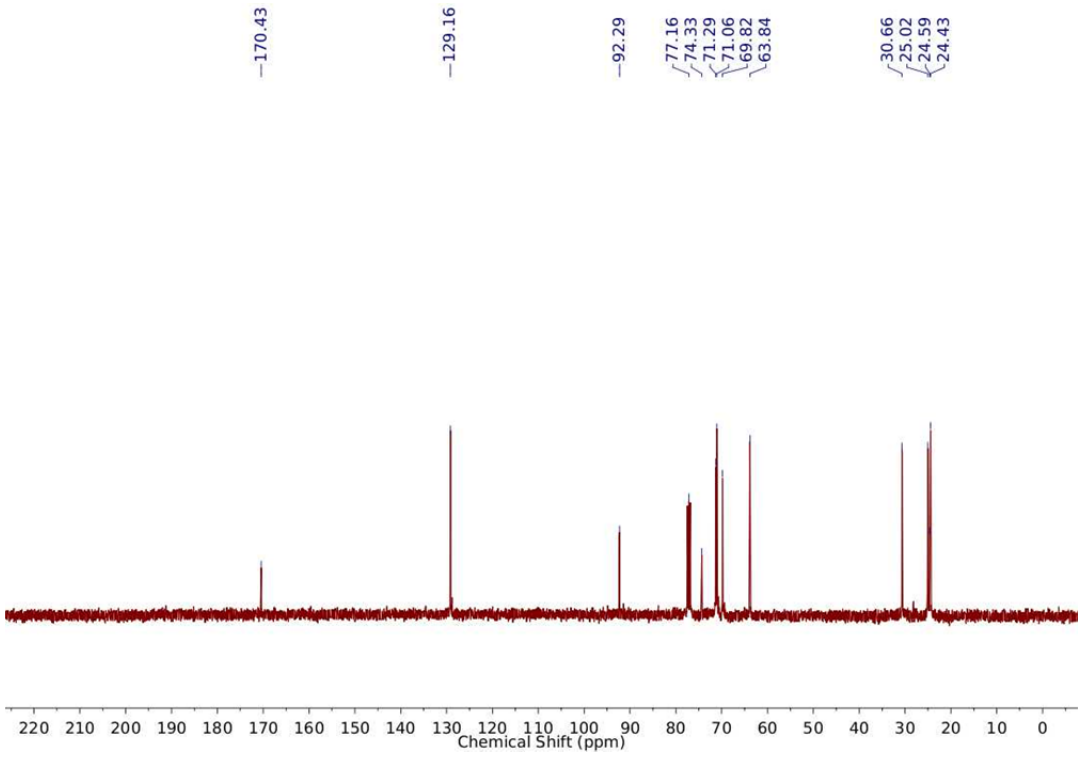

Figure 41. ^{13}C NMR spectrum of **6** in $CDCl_3$.

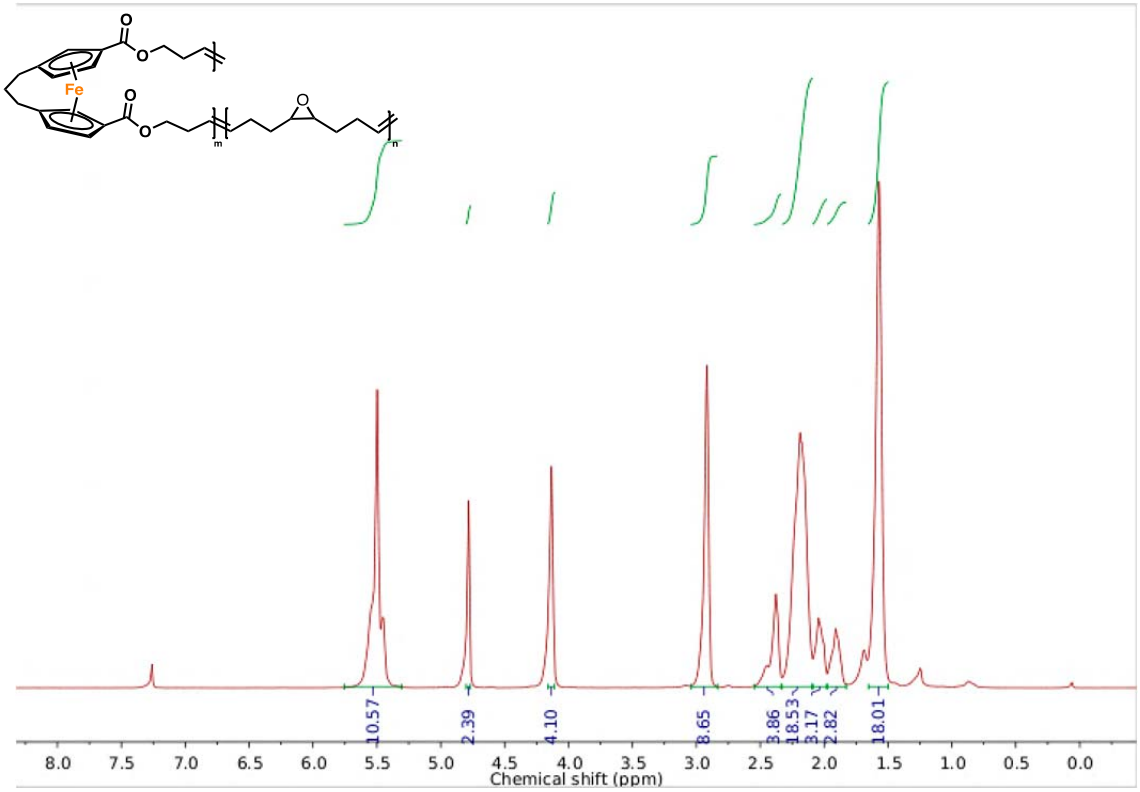

Figure 42. ^{1}H NMR spectrum of **7** (18% incorporation) in $CDCl_3$.

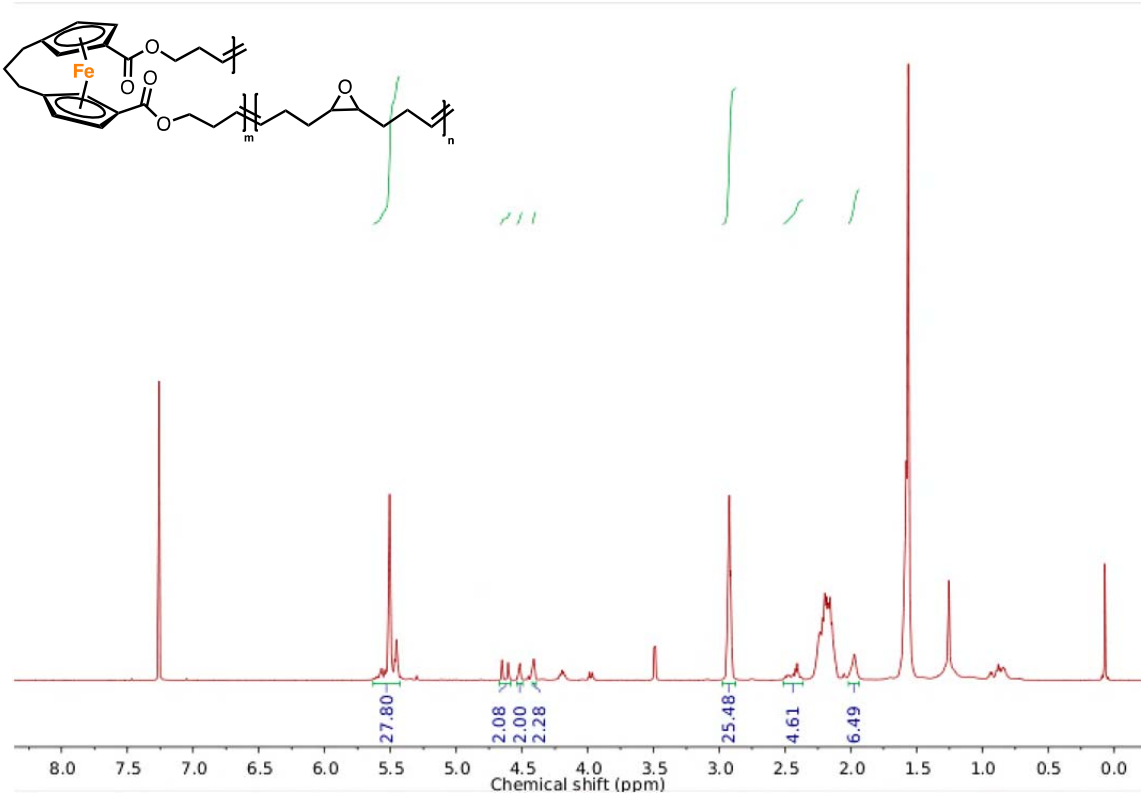

Figure 43. ^{1}H NMR spectrum of **8** (7% incorporation) in $CDCl_3$.

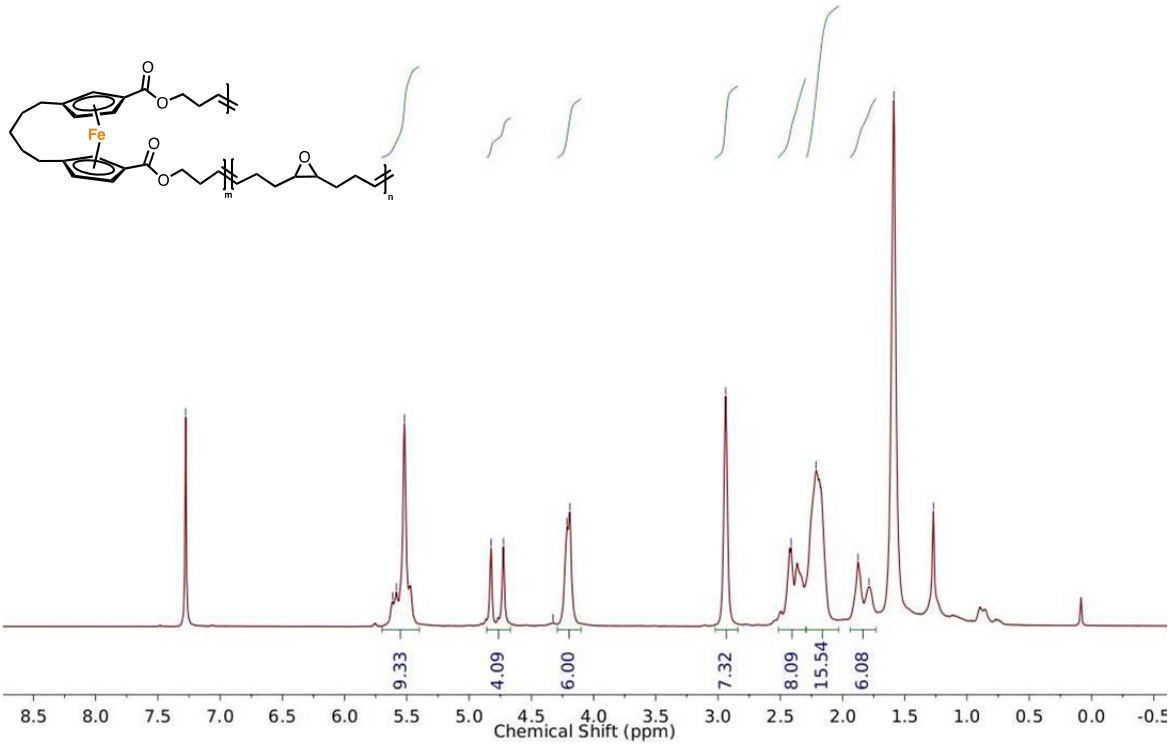

Figure 44. ^{1}H NMR spectrum of **9** (21% incorporation) in $CDCl_3$.

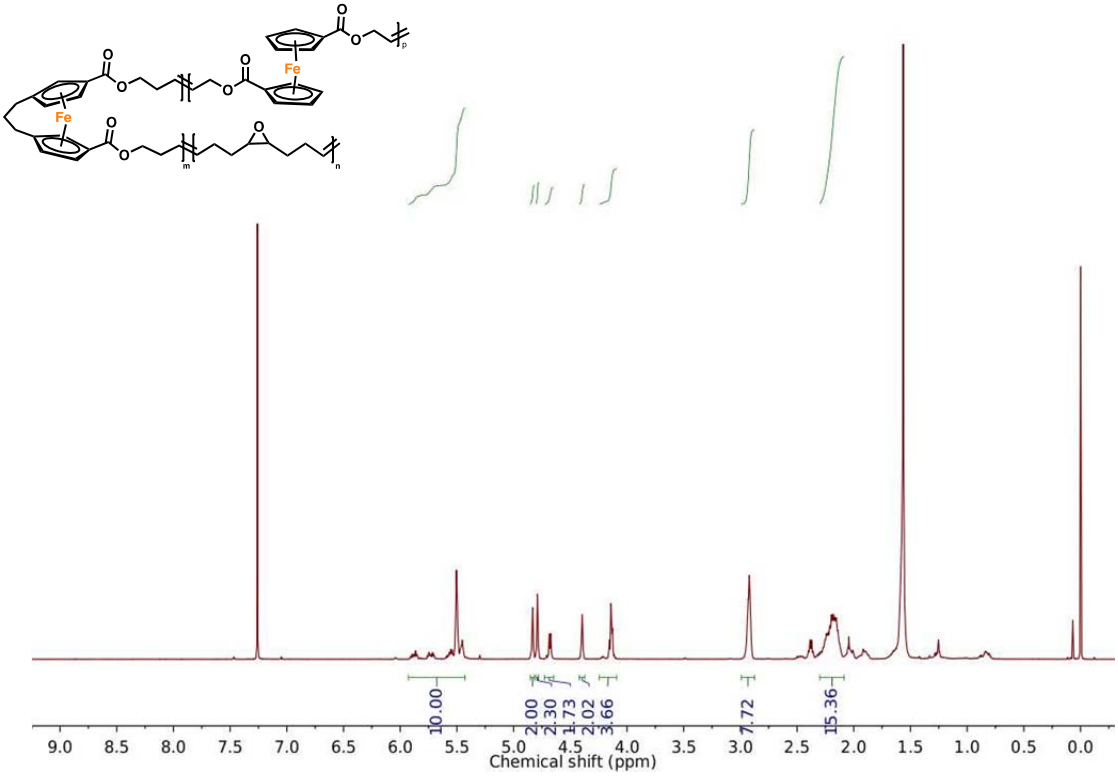

Figure 45. ^{1}H NMR spectrum of **10** (11% FC, 12% *cis*-3FCP) in $CDCl_3$.

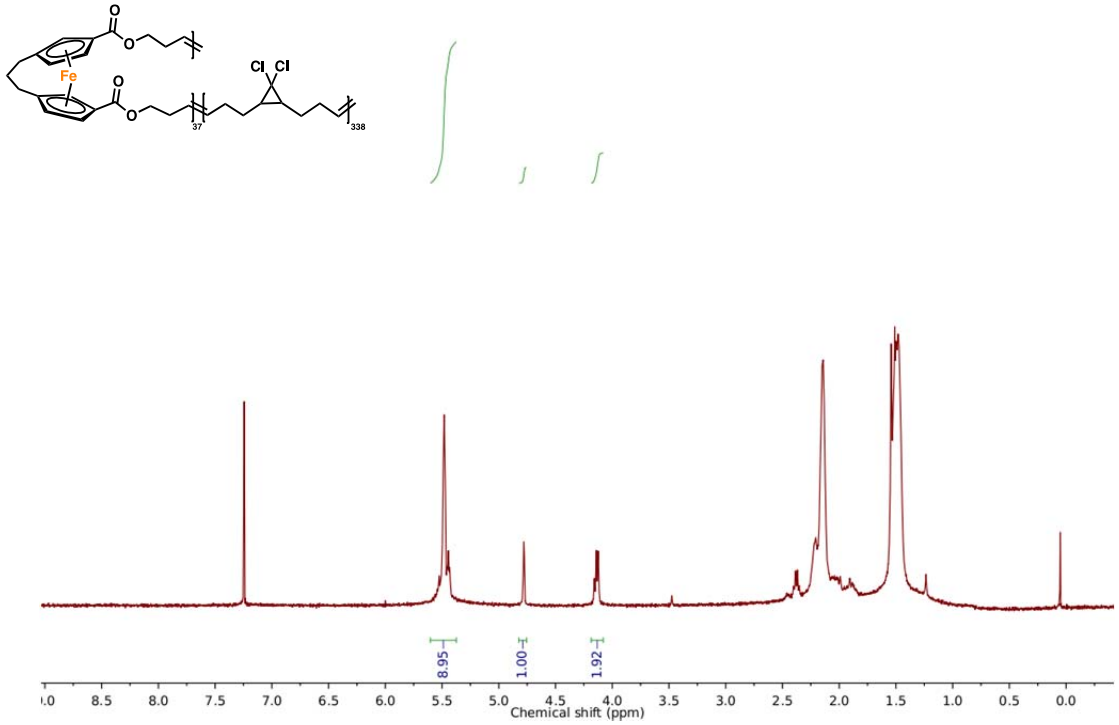

Figure 46. ^{1}H NMR spectrum of **11 (**11% incorporation**)** in $CDCl_3$.

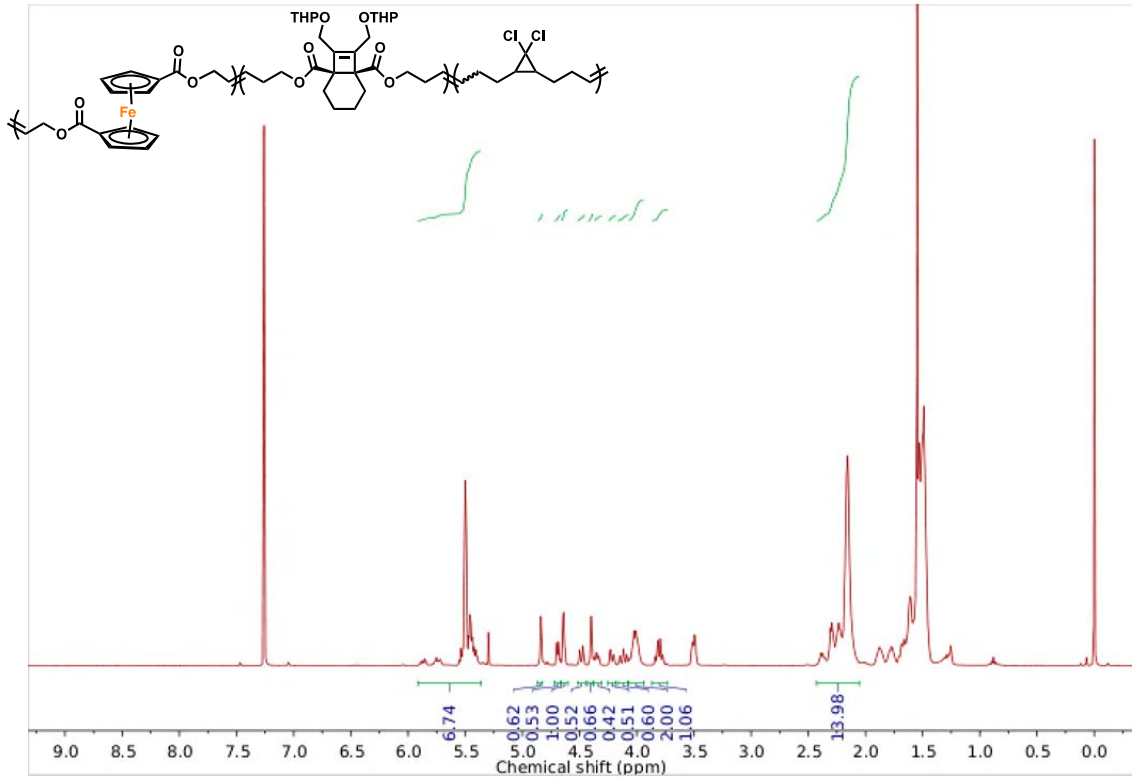

Figure 47. ^{1}H NMR spectrum of **12 (**5% FC, 15% BCOE**)** in $CDCl_3$.

11. References:

1 Turbitt, T. & Watts, W. Bridged ferrocenes: XII. The synthesis of [3] ferrocenophan-1-one from ferrocene by a novel one-step annelation reaction. *Journal of Organometallic Chemistry* **46**, 109-117 (1972).

2 Hisatome, M. & Hillman, M. Bridged ferrocenes: VII. Synthesis of di-and tri-bridged ferrocenes with pentamethylne chains. *Journal of Organometallic Chemistry* **212**, 217-231 (1981).

3 Kouznetsova, T. B., Wang, J. & Craig, S. L. Combined Constant□Force and Constant□Velocity Single□Molecule Force Spectroscopy of the Conrotatory Ring Opening Reaction of Benzocyclobutene. *ChemPhysChem* **18**, 1486-1489 (2017).

4 Wang, J. *et al.* Inducing and quantifying forbidden reactivity with single-molecule polymer mechanochemistry. *Nature chemistry* **7**, 323 (2015).

5 Gossweiler, G. R. *et al.* Mechanochemical Activation of Covalent Bonds in Polymers with Full and Repeatable Macroscopic Shape Recovery. *ACS Macro Letters* **3**, 216-219, doi:10.1021/mz500031q (2014).

6 Sha, Y. *et al.* Quantitative and Mechanistic Mechanochemistry in Ferrocene Dissociation. *ACS Macro Letters* **7**, 1174-1179 (2018).

7 Shannahan, L. *et al.* A Mechanochemistry-Based Technique For Early Material Damage Detection In High Strain Rate Processes. (ARMY RESEARCH LAB ABERDEEN PROVING GROUND MD ABERDEEN PROVING GROUND United …, 2019).

8 Hillman, M., Matyevich, L., Fujita, E., Jagwani, U. & McGowan, J. Bridged ferrocenes. 9. Lithiation and subsequent reactions of 1, 1'-trimethyleneferrocene. *Organometallics* **1**, 1226-1229 (1982).

9 Gossweiler, G. R., Kouznetsova, T. B. & Craig, S. L. Force-rate characterization of two spiropyran-based molecular force probes. *Journal of the American Chemical Society* **137**, 6148-6151 (2015).

10 Serpe, M. J. *et al.* A simple and practical spreadsheet-based method to extract single-molecule dissociation kinetics from variable loading-rate force spectroscopy data. *The Journal of Physical Chemistry C* **112**, 19163-19167 (2008).

11 E. S. Domalski, E. D. H., J. A. Martinho Simoes. (National Institute of Standards and Technology (NIST)).

12 Nelson, J. M., Rengel, H. & Manners, I. Ring-opening polymerization of [2] ferrocenophanes with a hydrocarbon bridge: synthesis of poly (ferrocenylethylenes). *Journal of the American Chemical Society* **115**, 7035-7036 (1993).

13 Siemeling, U., Krallmann, R., Jutzi, P., Neumann, B. & Stammler, H.-G. [3] Ferrocenophanes with a tetramethyldisiloxane bridge: Synthesis and molecular structure. *Monatshefte für Chemie/Chemical Monthly* **125**, 579-586 (1994).

14 Musgrave, R. A. *et al.* Main-chain metallopolymers at the static–dynamic boundary based on nickelocene. *Nature Chemistry* **9**, 743 (2017).

15 Gilroy, J. B. *et al.* An iron-cyclopentadienyl bond cleavage mechanism for the thermal ring-opening polymerization of dicarba [2] ferrocenophanes. *Chemical Science* **3**, 830-841 (2012).

16 Nelson, J. M. *et al.* Thermal Ring□Opening Polymerization of Hydrocarbon□ Bridged [2] Ferrocenophanes: Synthesis and Properties of Poly (ferrocenylethylene) s and Their Charge□Transfer Polymer Salts with Tetracyanoethylene. *Chemistry–A European Journal* **3**, 573-584 (1997).

17 Xu, J., Che, P. & Ma, Y. More sensitive way to determine iron using an iron (II)−1, 10-phenanthroline complex and capillary electrophoresis. *J. Chromatogr. A* **749**, 287-294 (1996).

18. Lin, Y., Kouznetsova, T. B., Chang, C. & Craig, S. L. Enhanced polymer mechanical degradation through mechanochemically unveiled lactonization. *Submitted*,